A Generalized Stress Parameter Approach for Fatigue Life Prediction of Seam Welded Joints

by

Xiao Wu

A thesis submitted in partial fulfillment
of the requirements for the degree of
Master of Science in Engineering
(Mechanical Engineering)
in the University of Michigan-Dearborn
2017

Master's Thesis Committee:

Professor Hong-Tae Kang, Chair
Professor Yi Zhang
Associate Professor German Reyes-Villanueva

ACKNOWLEDGEMENTS

I would like to give my greatest thanks to my supervisor, Professor Hong-Tae Kang, for his immense advice, support, and patience throughout my study and research period at UM-Dearborn. I have not only increased my knowledge in the field of durability under his guidance but also learned how to live and work better from his personality.

I am also grateful to Mr. Changjian Wei and Mr. Kejian Li for their assistance and company during these two years. I am pleased to have them as my colleagues and friends. Besides, I would like to thank all my friends who once encouraged and helped me. I wish them the best.

The financial support from Auto/Steel Partnership for this project is highly appreciated. This thesis would have not been possible without their support.

Finally, my special thanks belong to my parents, who stay behind me, support my decisions, and love me as always.

TABLE OF CONTENTS

LIST OF TABLES

LIST OF FIGURES

LIST OF ABBREVIATIONS

AHSS	advanced high strength steel
ESS	equivalent structural stress
FEA	finite element analysis
GMAW	gas metal arc welding
GSP	generalized stress parameter
SIF	stress intensity factor
SWT	Smith, Watson, and Topper mean stress correction equation
a	depth of semi-elliptical crack
a_i	initial crack depth
a_f	final crack depth
a/c	crack aspect ratio
b	fatigue strength exponent
c	half-length of semi-elliptical crack
C	fatigue crack growth coefficient
C'	fatigue strength coefficient
K	stress intensity factor
I	crack propagation integral
L	overall width of the welded attachment
m	fatigue crack growth factor

$m\left(x, \frac{a}{t}, \frac{a}{c}, \alpha\right)$	weight function
N	fatigue life
R	stress ratio
r or r_b	bending ratio
S	generalized stress parameter
S_s	equivalent structural stress
t	thickness of weldment
Y_m	geometric correction factor under tension
Y_b	geometric correction factor under bending
α	weld angle
Δ	range in cyclic loading ($\Delta K, \Delta Y, \Delta\sigma, \Delta S$)
ρ	weld toe radius
$\sigma(x)$	through-thickness normal stress distribution
σ_a	stress amplitude
σ_{ar}	fully reversed stress amplitude
σ_s	structural stress
σ_m	membrane component of structural stress
σ_b	bending component of structural stress
σ_{max}	maximum stress
σ_{min}	minimum stress
σ_{mean}	mean stress

ABSTRACT

This thesis presents a new method, based on fracture mechanics analysis of fatigue, to calculate the generalized stress parameter proposed by Maddox. The generalized stress parameter is computed from the currently existing structural stress definition and the stress intensity factor (SIF) calculation. With the structural stress term accounting for the effect of global weldment geometry, the stress intensity factor captures the local effect of the weld profile, characterized by the weld angle and weld toe radius. Parametric equations for the stress intensity factor are used to obtain the generalized stress parameter. A series of detailed two-dimensional finite element analyses, combined with the weight function method, is employed to validate the effectiveness of the utilized parametric equations. The validity range of these parametric equations is also extended to a wider range, i.e., a larger toe radius, which is more typical for current welded structures in the automotive industry. Finally, the generalized stress parameter is validated with fatigue test results of various specimen types and thickness combinations. It is found that the generalized stress parameter can adequately predict the fatigue life of welded joints and can serve as a better fatigue damage parameter than the structural stress since the weld profile effect has been included.

CHAPTER I

INTRODUCTION

1.1 Research background

Welded joints are widely found in the automotive, offshore, aircraft, and mechanical engineering industries to join separate components and structures [1]. Unfortunately, welds are often the weakest locations of the welded structures due to the highest stress concentration caused by the geometric discontinuity induced by the welding process and the altered material properties, especially under fatigue loading conditions. Thus, it is necessary for engineers and researchers to understand the fatigue characteristics of the welded joints and develop accurate methods to estimate their fatigue lives. However, many factors can affect the fatigue strength of the welded joints and can make the life prediction complicated and inaccurate.

According to the geometry of the welds, the welded joints can be divided into two groups: seam welded joints and spot welded joints. In spot welded joints, the weld shape looks like a "spot," which is produced in the welding process to melt the metal, form the weld and connect the parts. Contrary to the spot weld, a seam weld is a continuous line welds, which can be formed by various welding techniques, e.g., laser welding and gas metal arc welding, etc. With lots of efforts have been put on the analysis of spot welded joints [2-8], this thesis mainly focuses on the fatigue analysis of seam welded joints. However, it should be noted that the approach proposed in this study may also be applied on spot welds if following a certain modeling technique as discussed in [9].

For either seam welded joints or spot welded joints, the welding process will intensely affect the materials by the process of heating and subsequent cooling, as well as the fusion process resulting in the inhomogeneous material property. Furthermore, some defects, such as inclusions, pores, and cavities, are usually generated in the welding process, which can cause high stress concentration decreasing the fatigue strength of the joints. Residual stress and distortions induced in the welding process will also affect the fatigue behavior. All these facts will contribute to the complexity of the fatigue life predictions of the joints. So, it is not surprising that none of the existing methods can consider these effects at the same time.

In addition to the above factors, it is also acknowledged that the fatigue performance of welded structures is closely related to the geometry of the welds and weldments, e.g., weld angle, weld toe radius, and thickness of the weldments, etc. [10]. However, the effects of the local geometries are only partially considered in the traditional fatigue design and analysis rules of welded joints, which use stress-life (S-N) curves. The experimental generation of these S-N curves is usually based on the assumption of "normal" quality welds, and the variety of geometries constitutes one of the main reasons for the large scatters happening in S-N curves. While the scatter can be reduced by using finite element analysis (FEA) to model the details of the weld profile with very fine meshes, it is impossible to do that on actual welded structures, which may have hundreds of welds.

Structural stress concepts with different definitions have been proposed by many researchers in attempts to overcome this difficulty [11-14]. Among them, the nodal force-based structural stress definition [11, 12] may be the most widely accepted and implemented one in the engineering industries. It claims the advantage of mesh-insensitivity, so that coarse meshes can be used to significantly reduce the time of FEA simulations for large structures [8, 9]. Based on the

theory of elementary structural mechanics, nodal force-based structural stress works as the "nominal stress" in the welded joints and takes the global geometric effect of the weldments into account, but the local geometric effect introduced by the weld profile is still lacking consideration and demands to be analyzed.

The fracture mechanics approach is another attractive and helpful way to analyze the fatigue failure and predict the fatigue life of welded joints and structures from the perspective of crack initiation and crack propagation [2, 15]. In the regime of fracture mechanics, one of the most important parameters is the stress intensity factor (SIF), which is a parameter used to describe the stress state ("stress intensity") caused by external loads near the crack tip. It can be utilized solely as a fatigue damage parameter to correlate the fatigue life [2] or be combined with Paris' Law [16] to integrate the total fatigue life [15]. However, the analytical solutions for SIF calculation are available only for simple geometries; for complex geometries, FEA should be employed to calculate the SIFs, which is time-consuming due to the requirements of accurate fatigue crack description and a fine mesh. In many alternative endeavors to determine the SIFs, the weight function method [17-21] has proved to be an efficient approach by using the stress distribution on the un-cracked cross-section of the welded body, thus avoiding detailed simulation of the crack. Furthermore, the weight function method has been employed by Brennan et al. [22] to formulate parametric equations for stress intensity factors of T-butt welded joints, along with conducting a comprehensive set of two-dimensional FEA simulations. These parametric equations provide the capability for a faster calculation of SIFs; however, its ability is limited to a particular validity range based on the simulation carried out by Brennan et al., which had a small weld toe radius compared to the plate thickness ($0.01 \leq \rho/t \leq 0.066$). In many cases, especially in automotive industries, thin sheets are often used and welded together, which will form a large weld toe radius

compared to its sheet thickness ($0.066 \leq \rho/t \leq 0.5$). Under this circumstance, the effectiveness of Brennan's parametric equations for SIFs must be investigated before they are directly applied to estimate the fatigue life for these welded thin sheets and welded joints.

In this study, the parametric equations for SIFs calculation are first validated by comparing them to the corresponding SIF results obtained from the detailed FEA simulation and the weight function method for the cases of large weld toe radii. Then the parametric equations for SIFs are combined with the structural stress method to form the "generalized stress parameter" proposed by Maddox [23]. With the structural stress term accounting for the effect of global weldment geometry, the inclusion of SIF (or equivalent "geometric correction factor") captures the local effect of the weld profile characterized by the weld angle and weld toe radius. Finally, the obtained generalized stress parameter is validated with fatigue test results of various specimen types and thickness combinations. It is found that the generalized stress parameter is able to predict the fatigue life of welded joints accurately and can serve as a better fatigue damage parameter than the structural stress.

1.2 Current status of the fatigue analysis methods of seam welded joints

It is known that welded joints are ubiquitous in many industries and are usually the failure locations under fatigue loads. In the early design phase, it is required to have a knowledge about their fatigue behavior and an estimated service life. Considering the importance and complexity of this subject, numerous efforts have been put in the method development for fatigue analysis and life assessment. In this section, two commonly used methods, along with their respective variants, will be introduced in detail. These methods also constitute the foundation of the new approach that will be described in the following chapters.

1.2.1 Structural stress method

Structural stress methods have been developed recently based on the elementary structural mechanics' theory. The structural stress is defined as the nominal stress at the weld toe or weld root cross-section, which neglects the local geometric effect caused by the weld profile. As shown in Figure 1.1 [12], by considering the force and moment equilibrium condition for the local stress distributions, the structural stress can be decomposed into a membrane component σ_m and a bending component σ_b:

$$\sigma_s = \sigma_m + \sigma_b \tag{1.1}$$

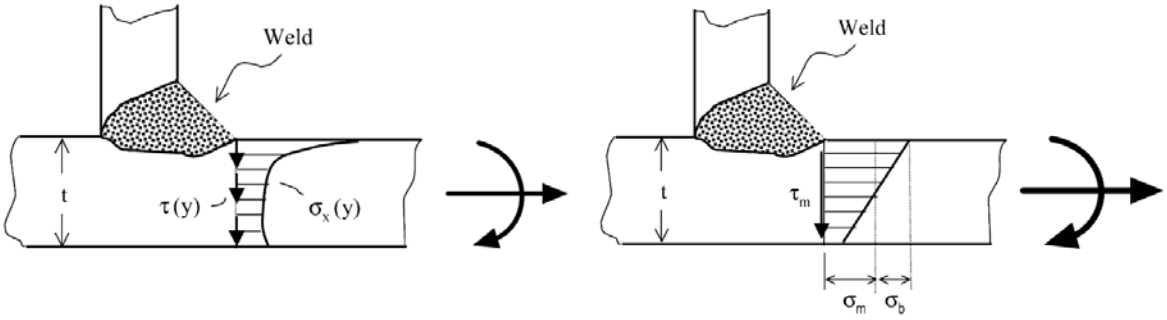

(a) (b)

Fig. 1.1 (a) Local stress distribution and (b) Structural stress distribution

Based on the above definition, the structural stress can be calculated either from solid element model or shell element model. When using solid element model, the through-thickness normal stress distribution can be used to calculate the membrane component σ_m and bending component σ_b to compute the final structural stress σ_s. In comparison to the solid model, shell element model is more preferred in modelling the welded joints since the thicknesses of these joints are usually very thin comparing to the other dimensions, under which case using shell element is more efficient and time-saving. Furthermore, when the shell element model is used, the

structural stress can be calculated from the nodal forces and nodal moments, which are believed to be mesh-insensitive. It means the structural stress value will be less dependent on or independent of the mesh size, which helps to avoid the stress singularity phenomenon that happens often in the welded joint cases. By using the shell element model, Eq. (1.1) can be further written as:

$$\sigma_s = \sigma_m + \sigma_b = \frac{f_x}{t} + \frac{6m_y}{t^2} \tag{1.2}$$

As can be shown in Figure 1.2 [12], f_x and m_y are the line force and line moment, respectively, and t is the element thickness.

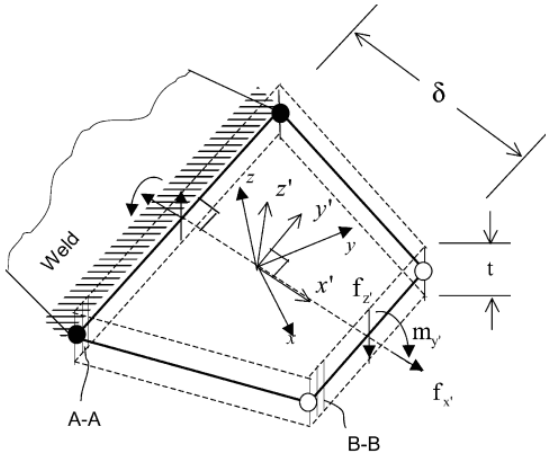

Fig. 1.2 Line force and line moment on a shell element

Eq. (1.2) shows that the information about line forces/moments is required in order to calculate the structural stress. They are actually extracted from the nodal forces and nodal moments, which are direct FEA outputs in most of the commercial software. The procedure to calculate the line forces/moments from nodal forces/moments is called "line force recovery" or "structural stress recovery" method. The following part will introduce three different structural stress approaches, in which different line force recovery methods are implemented.

1.2.1.1 Fermer's approach

Fermer and his co-workers [11] proposed a structural stress method, along with a stress recovery process, by assuming that the line force/moment to be linearly distributed along the element length. Sometimes, this approach is also called as the "Volvo method" [24]. The line force/moment and the nodal force/moment have the following relation (see Fig. 1.3 [25]):

$$f_x^{(i)}(y) = \frac{2}{l_y^{(i)}}\left(F_{x1}^{(i)}\left(1 - \frac{y}{l_y^{(i)}}\right) + F_{x2}^{(i)}\frac{y}{l_y^{(i)}}\right) \tag{1.3}$$

$$m_y^{(i)}(y) = \frac{2}{l_y^{(i)}}\left(M_{y1}^{(i)}\left(1 - \frac{y}{l_y^{(i)}}\right) + M_{y2}^{(i)}\frac{y}{l_y^{(i)}}\right) \tag{1.4}$$

where $f_x^{(i)}(y)$ and $m_y^{(i)}(y)$ are the line force and line moment, respectively, on the i^{th} element. $F_{x1}^{(i)}$ and $F_{x2}^{(i)}$ are the nodal forces applied at the nodes of the i^{th} element. $M_{y1}^{(i)}$ and $M_{y2}^{(i)}$ are the nodal moments applied at the nodes of the i^{th} element, $l_y^{(i)}$ is the edge length of the i^{th} element and y is the coordinate, which shows the weld line direction.

Then, the structural stress at each node ($\sigma_{s,1}^{(i)}$ and $\sigma_{s,2}^{(i)}$) on the i^{th} element can be calculated using the following equations:

$$\sigma_{s,1}^{(i)} = \frac{2F_{x1}^{(i)}}{l_y^{(i)}t} + \frac{12M_{y1}^{(i)}}{l_y^{(i)}t^2} \tag{1.5}$$

$$\sigma_{s,2}^{(i)} = \frac{2F_{x2}^{(i)}}{l_y^{(i)}t} + \frac{12M_{y2}^{(i)}}{l_y^{(i)}t^2} \tag{1.6}$$

By examining the Fig. 1.3, it can easily be found that at each shared node inside a continuous weld, there will be two structural stresses. In this situation, the larger of the two stress values shall be used for fatigue life assessment of the weld.

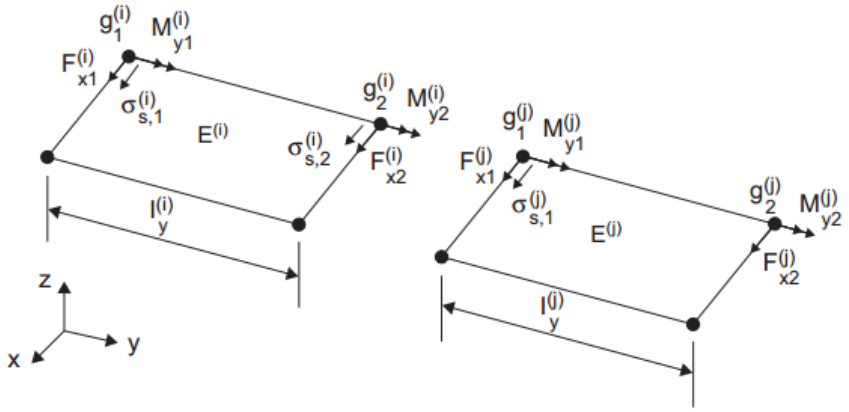

Fig. 1.3 Structural stresses and nodal forces/moments distribution on adjacent elements

1.2.1.2 Modified Fermer's approach

Fermer's approach was later modified by nCode DesignLife [26], which is now called as the "modified Fermer's approach" or "nCode structural stress method" [24, 27]. It has wider application compared to the original method. The steps to calculate the structural stresses from the nodal forces/moments are listed below, with an example of two-element case (see Fig. 1.4):

1. Reallocate the (total) nodal force at the shared node in proportion to the element edge length

$$F_2^{Left} = F_2 \frac{l_1}{l_1+l_2} \qquad F_2^{Right} = F_2 \frac{l_2}{l_1+l_2} \tag{1.7}$$

2. Calculate the line forces/moments using the equilibrium condition on each element

$$f_1 = \frac{2}{l_1}\left(2F_1 - F_2^{Left}\right) \quad f_2^{Left} = \frac{2}{l_1}\left(2F_2^{Left} - F_1\right) \tag{1.8}$$

3. Take the average of the line forces on each element to get the value at the middle of the element edge

$$f_{E1} = \frac{1}{2}\left(f_1 + f_2^{Left}\right) \tag{1.9}$$

4. Calculate the structural stress at the middle of the element edge using the averaged line forces and line moments

$$\sigma_{E1} = \frac{f_{E1}}{t} + \frac{6m_{E1}}{t^2} \tag{1.10}$$

Note that the line moment m_{E1} can be obtained similarly as the line force f_{E1} through steps 1-3. F_1, F_2 and F_3 are the (total) nodal forces at each node, F_2^{Left} and F_2^{Right} are the component nodal forces at the shared node, f_1 and f_2^{Left} are the line forces on the left element, l_1 and l_2 are the element edge lengths.

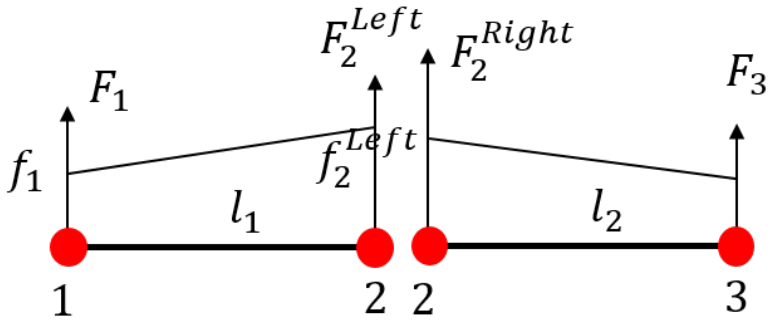

Fig. 1.4 Line forces and nodal forces distribution on adjacent elements in a two-element case

By following similar steps, a matrix relationship between the averaged line forces/moments and the nodal forces/moments can be obtained for an n-element case. The matrix relationship can simply be summarized as

$$[f] = [T][F] \quad [m] = [T][M] \tag{1.11}$$

where $[f]$ and $[F]$ are the line force vector and nodal force vector, respectively. $[m]$ and $[M]$ are the line moment vector and nodal moment vector, respectively. And $[T]$ is the transformation

matrix. Therefore, the structural stress can then be calculated from the nodal forces/moments using Eq. (1.10) and Eq. (1.11).

Though the structural stress has taken the global geometric effect into consideration, it is acknowledged that the thickness of the plates has an additional effect on the fatigue strength. Thus, in modified Fermer's approach, a thickness correction term is added by applying a factor $f(t)$ onto the above obtained structural stress. The thickness correction factor $f(t)$ is determined as

$$f(t) = 1 \quad if\ t < T_{ref} \tag{1.12}$$

$$f(t) = (\frac{t}{T_{ref}})^{\frac{1}{6}} \quad if\ t \geq T_{ref} \tag{1.13}$$

where T_{ref} is the reference thickness and its default setting is 1 mm in nCode designLife [26].

1.2.1.3 Dong's approach

Dong and his coworkers [12, 28-31] proposed a so called "equivalent structural stress method" based on the prior structural stress definition and the fracture mechanics consideration. This approach was later implemented into commercial FEA software Fe-safe, so it is also called "Fe-safe structural stress method" or "Battelle structural stress method."

To calculate the equivalent structural stress, the first step is to recover the structural stress from the nodal forces/moments. This procedure is carried out with an assumption that the work done by the nodal forces/moments is equal to the work done by the line forces/moments. Under this assumption, like the modified Fermer's approach, there is another matrix relationship between the nodal forces/moments and line forces/moments, which can be expressed as:

$$[F] = [L][f] \quad [M] = [L][m] \tag{1.14}$$

where $[L]$ is the transformation matrix in Dong's approach. By using the inverse of $[L]$, line forces $[f]$ and line moments $[m]$ can be computed from the nodal forces and nodal moments. Then Eq. (1.2) can be employed to calculate the structural stress σ_s.

The second step is to derive the equivalent structural stress based on the fracture mechanics considerations. It originates from the well-known Paris' Law:

$$\frac{da}{dN} = C(\Delta K)^m \tag{1.15}$$

where a is the crack depth, N is the fatigue life, C and m are the material parameters, and ΔK is the stress intensity factor range.

Based on the observations of anomalous crack growth on the historical data, Dong postulated that if a sharp notch is considered, instead of using a monotonic stress intensity factor to describe the fatigue crack growth behavior, non-monotonic K as a function of crack size can be developed near the notch tip so that the crack growth behavior between short crack (notch tip) regime and long crack regime could be treated distinguishably, as shown in Fig. 1.5 [30]. Thus, founded on these facts, Dong proposed a two-stage growth model [30], which is expressed as:

$$\frac{da}{dN} = C(\Delta K_{notch})^n(\Delta K)^{m-n} \tag{1.16}$$

where ΔK_{notch} is the notch stress intensity factor range characterizing the crack growth behavior from $0 < a/t < 0.1$ (small crack) and ΔK is the far field stress intensity factor range characterizing the crack growth behavior from $0.1 \leq a/t \leq 1.0$ (long crack) in cyclic loading conditions. Here, $\frac{a}{t} = 0.1$ is approximately taken as the boundary between these two regimes based on the experimental observations on historical data. n is another material parameter

determined based on the crack growth data covering both typical short crack and long crack regimes.

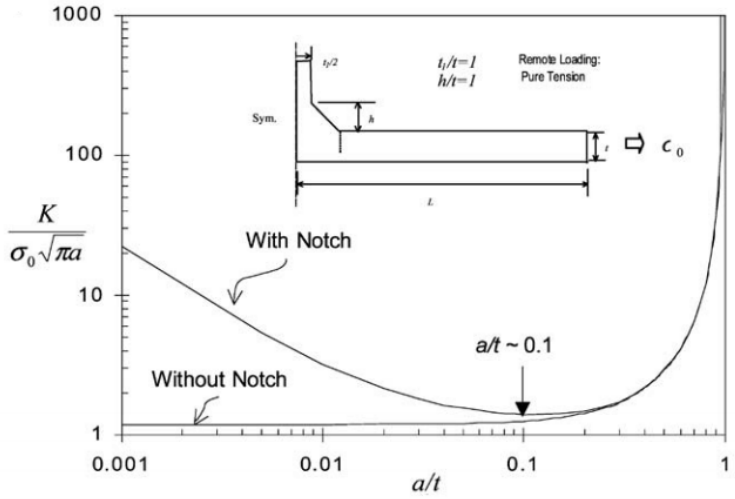

Fig. 1.5 Stress intensity changes as a function of crack size a/t for a notched specimen under remote tension

By virtue of the stress intensity magnification factor (M_{kn}) concept, Eq. (1.16) can be further modified as

$$M_{kn} = \frac{\Delta K_{notch}}{\Delta K} \tag{1.17}$$

$$da = C(M_{kn})^n(\Delta K)^m dN \tag{1.18}$$

The fatigue life can be estimated by integrating the Eq. (1.18) as

$$N = \int dN = \int \frac{t}{C(M_{kn})^n(\Delta K)^m} d\left(\frac{a}{t}\right) \tag{1.19}$$

Eq. (1.19) shows that in order to estimate the fatigue life, the determination of the stress intensity factor range ΔK is necessary. It has been shown [30] that ΔK for complex geometry under complex loading mode can be calculated from ΔK for a simple geometry under simple far field loading. This transformation tells that the stress intensity factor can be related to the structural

stress concept, which actually works as the far field stress equivalently. For example, considering an edge crack case, the ΔK for mode I can be expressed as:

$$\Delta K = \Delta K_m + \Delta K_b = \sqrt{t}\left(\Delta\sigma_m f_m\left(\frac{a}{t}\right) + \Delta\sigma_b f_b\left(\frac{a}{t}\right)\right)$$

$$= \Delta\sigma_s\sqrt{t}\left[f_m(\frac{a}{t}) - r\left(f_m(\frac{a}{t}) - f_b(\frac{a}{t})\right)\right] \tag{1.20}$$

where $r = \Delta\sigma_b/\Delta\sigma_s$ is the bending ratio. ΔK_m and ΔK_b are the stress intensity factor range under pure membrane loading and pure bending loading respectively. $f_m(\frac{a}{t})$ and $f_b(\frac{a}{t})$ are dimensionless functions of relative crack size a/t for the membrane component and bending component of the far field stress (structural stress) state. For the edge crack case, the expressions for $f_m(\frac{a}{t})$ and $f_b(\frac{a}{t})$ can be found in the literature [32]. For the semi-elliptical crack case, a relationship similar to Eq. (1.20) holds between the stress intensity factor range and the structural stress range, and can be found in [33]. For the sake of simplicity, the elaboration of Dong's approach will be demonstrated on the case of edge crack, but it is also applicable for the semi-elliptical crack case.

With the substitution of Eq. (1.20) into Eq. (1.19), a new equation can be established as:

$$N = \frac{1}{C}\cdot t^{1-\frac{m}{2}}\cdot(\Delta\sigma_s)^{-m}\cdot\int\frac{1}{(M_{kn})^n(\left[f_m(\frac{a}{t})-r\left(f_m(\frac{a}{t})-f_b(\frac{a}{t})\right)\right])^m}d\left(\frac{a}{t}\right)$$

$$= \frac{1}{C}\cdot t^{1-\frac{m}{2}}\cdot(\Delta\sigma_s)^{-m}\cdot I(r) \tag{1.21}$$

or,

$$\Delta\sigma_s = C^{-\frac{1}{m}}\cdot t^{\frac{2-m}{2m}}\cdot I(r)^{\frac{1}{m}}\cdot N^{-\frac{1}{m}} \tag{1.22}$$

where $I(r) = \int \frac{1}{(M_{kn})^n \left(\left[f_m\left(\frac{a}{t}\right) - r_b\left(f_m\left(\frac{a}{t}\right) - f_b\left(\frac{a}{t}\right)\right)\right]\right)^m} d\left(\frac{a}{t}\right)$ is an integral and can be derived by carrying out the integration of above expression.

By rearranging Eq. (1.22), Dong defined the so called "equivalent structural stress parameter" [29] as:

$$\Delta S_s = \frac{\Delta\sigma_s}{t^{\frac{2-m}{2m}} \cdot I(r)^{\frac{1}{m}}} \tag{1.23}$$

The term $t^{\frac{2-m}{2m}}$ can be treated as the additional thickness correction and the integral term $I(r)^{\frac{1}{m}}$ accounts for the loading mode effect. It can be seen that the values of $I(r)^{\frac{1}{m}}$ are required to be obtained before the calculation of the equivalent structural stress. Numerical integrations are carried out on the expression of $I(r)^{\frac{1}{m}}$ with $m = 3.6$ and $n = 2$ for steel, and the results are fitted to polynomial functions in [31] as:

$$I(r)^{\frac{1}{m}} = 0.0011r^6 + 0.0767r^5 - 0.0988r^4 + 0.0946r^3 + 0.0221r^2 + 0.014r + 1.2223 \tag{1.24}$$

$$I(r)^{\frac{1}{m}} = 2.1549r^6 - 5.0422r^5 + 4.8002r^4 - 2.0694r^3 + 0.561r^2 + 0.0097r + 1.5426 \tag{1.25}$$

Note that Eq. (1.24) is obtained under the load-controlled conditions, and Eq. (1.25) is obtained under the displacement-controlled conditions. Using Eq. (1.23)-Eq. (1.25), the equivalent structural stress can then be calculated.

1.2.2 Fracture mechanics method

Fracture mechanics method usually refers to the class of methods which estimate the fatigue life by considering the crack propagation process and attempts to model the whole fatigue process by considering the influence of all significant parameters. Instead of using the stress or strain, the fracture mechanics method uses a variable known as the stress intensity factor (SIF), which is the combination of the stress and the geometry. The stress intensity factor range, ΔK, is the most important parameter governing the fatigue crack growth.

1.2.2.1 Stress intensity factor

The stress intensity factor, K, was first introduced by Irwin [34]. It was pointed out that when the SIF reaches a certain critical value beyond its "fracture toughness", instant facture will happen for a cracked body. Later on, it was found that the fatigue crack propagation behavior can be described in terms of crack growth rate da/dN plotted against the stress intensity factor range ΔK, also known as the fatigue crack growth curve (see Fig. 1.6 [35]).

The central portion of the crack growth curve (Region II) is linear in the log-log scale. The behavior in the central portion is commonly described by the crack growth equation proposed by Paris and Erdogan [16], which is popularly known as the Paris' law. As has been shown in Section 1.2.1.3, its simplest form is expressed as:

$$\frac{da}{dN} = C(\Delta K)^m \tag{1.15}$$

Note that the Paris' law only represents the linear phase (Region II) of the crack growth curve. As the stress intensity factor range increases approaching its critical value of fracture toughness (K_c), the fatigue crack growth rate becomes much faster and the cracked body will fracture soon in Region III and the cycles accumulated in this region can usually be negligible.

Therefore, the total life of an object under fatigue loading can be divided into two parts: crack initiation phase, and propagation phase. However, when it comes to the case of welded joints or welded structures, a pre-existing initial crack can be assumed based on the fact that a small gap is often formed artificially during the welding process to join different parts, and the initiation fatigue life is sometimes not considered. It means that the crack propagation life dominates the total fatigue life in welded joints. Under this case, the fatigue life can be estimated by integrating Eq. (1.15) from the initial crack size to the final crack size, given as:

$$N = \frac{1}{C}\int_{a_i}^{a_f}(\Delta K)^{-m}da \tag{1.26}$$

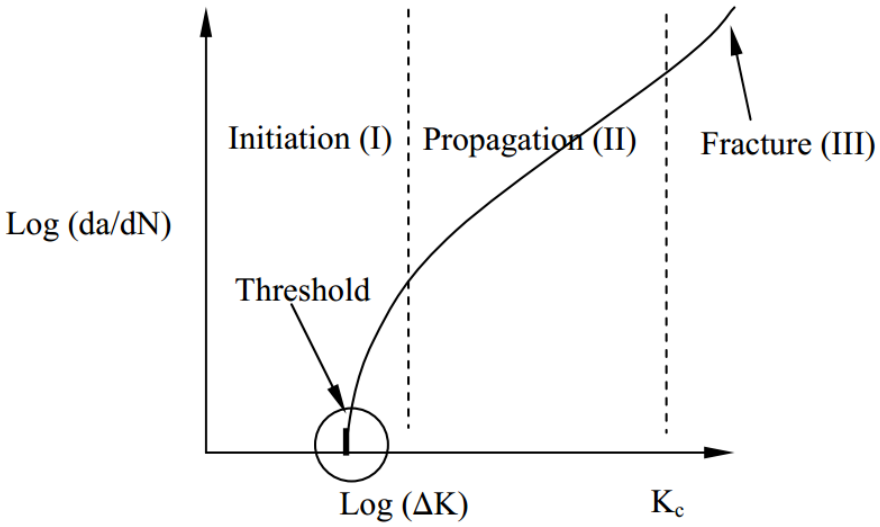

Fig. 1.6 Typical fatigue crack growth rate curve

There are three modes of loading that a crack can experience, as Fig. 1.7 shows [35]. Mode I loading, where the load is applied normal to the crack plane, tending to open the crack. Mode II corresponds to the in-plane shear loading and tends to slide one crack face with respect to the other. Mode III refers to the out-of-plane shear loading. A cracked body can be loaded in any one of these modes, or a combination of two or three modes. When different modes are considered, the stress

intensity factors should be used with subscripts, e.g. K_I, K_{II} and K_{III}, to distinguish different facture modes.

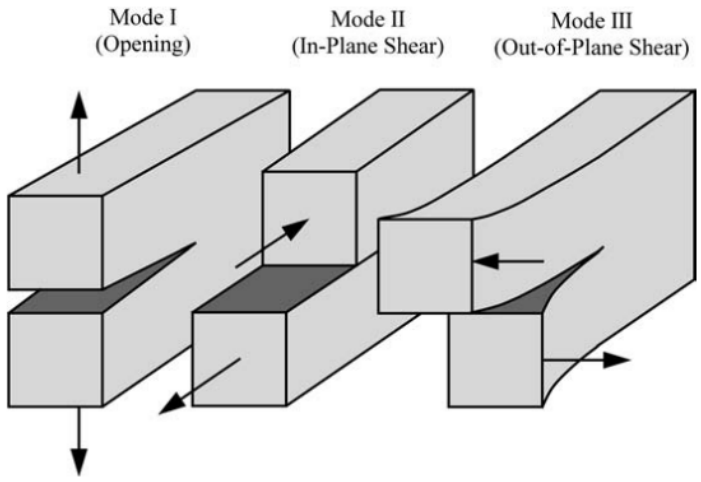

Fig. 1.7 Three typical loading modes that a crack can experience

1.2.2.2 Finite element simulation of fatigue crack growth

As can be seen in Eq. (1.26), the fatigue life can be estimated by carrying out the integration process, as long as the SIF ranges are known for the corresponding crack length. For welded joints, there is no analytical solution for SIF's calculation, so finite element analysis (FEA) is usually utilized to simulate the fatigue crack growth procedure. Very fine and regular meshes are required to model the crack and its surroundings adequately. The total length between the initial crack size and the final crack size should be divided into small segments. For each given crack size, the corresponding SIF ranges can be obtained by conducting the finite element simulation. By doing this, the numerical integral in Eq. (1.26) can be performed by using its incremental form, e.g.,

$$N = \frac{1}{C}\left[\int_{a_i}^{0.025a_f}(\Delta K(a))^{-m}da + \int_{0.025a_f}^{0.05a_f}(\Delta K(a))^{-m}da + \cdots + \int_{0.975a_f}^{a_f}(\Delta K(a))^{-m}da\right] \quad (1.27)$$

where $\Delta K(a)$ is changing with the crack depth a. Note that ΔK could be K_I, K_{II}, K_{III} or their combination depending on the fracture mode the cracked body endures.

1.2.2.3 Weight function method for SIF calculation

While FEA can be used to simulate the crack propagation procedure and calculate the SIF, it is time-consuming with respect to the efforts required for the crack modeling and is hard to apply to complex geometries. An alternative way is to use the weight function method [17, 18], which only requires the normal stress distribution for un-cracked bodies. The SIF can be calculated in such a way:

$$K = \int_0^a \sigma(x) m(x, a) dx \tag{1.28}$$

where $\sigma(x)$ is the normal stress distribution on the cross-section at the critical point of the un-cracked body, see Fig. 1.8 [21], and can be extracted from 2-D or 3-D FEA models. And $m(x, a)$ is the weight function and has been documented in many literatures for various geometries.

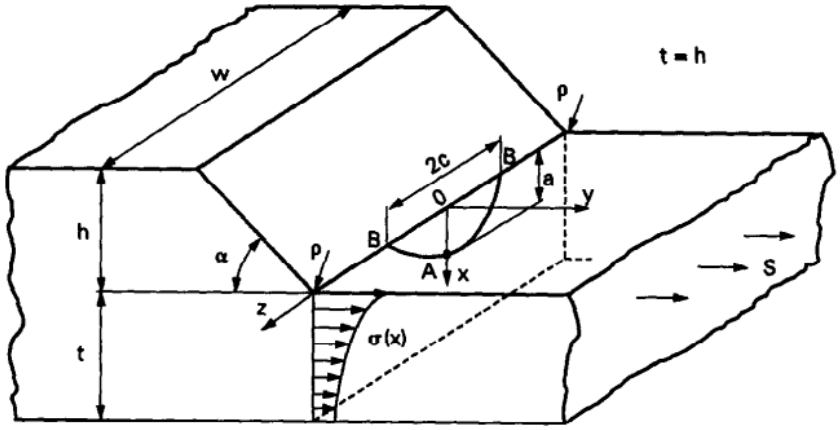

Fig. 1.8 Normal stress distribution in a weldment with a surface semi-elliptical crack

For example, Bueckner [18] and Newman et al. [36] have derived the weight functions for edge crack and surface semi-elliptical crack in finite thickness plate, respectively. Niu and Glinka

[19, 20] developed the weight functions for edge and surface semi-elliptical cracks in flat plates and plates with corners using 2-D FEA models, which considered the effects of weld profile geometry factors on local stress intensity factor evaluation. The disadvantage of the weight function method is that massive calculation is needed to conduct the numerical integrations.

1.3 Outline of the thesis

In this study, the "generalized stress parameter" concept proposed by Maddox [23] is used to assess the fatigue life of welded joints. The generalized stress parameter combines the structural stress method and fracture mechanics method. It requires the calculation of SIF. Instead of using the finite element method or weight function method, Brennan's parametric equations [22] are employed to provide fast calculation.

The limitation of Brennan's equations is that they have a requirement for the dimensions of the welded joints. After measuring the investigated welded joints in this study, it was found that the size of the weld toe radius is out of its claimed validity range. Thus, the parametric equations for SIFs calculation are first validated in Chapter II by comparing them to the results from the weight function method. Then, in Chapter III, the parametric equations for SIFs combined with the structural stress method are used to form the generalized stress parameter method. With the structural stress term accounting for the effect of global weldment geometry, the inclusion of SIF captures the local effect of the weld profile characterized by the weld angle and weld toe radius. A detailed scheme to calculate the generalized stress parameter from the structural stress and the weldment geometries is proposed for a large range of weld toe radii and weld angles. Chapter IV presents the experimental fatigue life test results, and the validation of the proposed methodology using the fatigue test results. Various specimen types and thickness combinations are investigated, and good prediction results are produced using the proposed method. It shows the generalized

stress parameter may have the potential to serve as a better fatigue damage parameter than the widely used structural stress. Chapter V summarizes the work completed and the conclusion made in this study.

CHAPTER II

PARAMETRIC EQUATIONS FOR STRESS INTENSITY FACTORS

2.1 Introduction

As mentioned in Chapter I, structural stress method considers only the global geometric effect. To take the local geometric effect into consideration, e.g., weld angle effect and weld toe radius effect, one practical solution is to use the stress intensity factor. It has been shown in [30, 37], the stress intensity factor can be related to the structural stress in the form of

$$K = (Y_m \sigma_m + Y_b \sigma_b)\sqrt{\pi a} \tag{2.1}$$

where Y_m and Y_b are geometric correction factors under pure tension and pure bending loading, respectively. σ_m and σ_b are the membrane component and the bending component of structural stress at the potential crack initiation location, respectively, and can be decomposed from the structural stress σ_s with the bending ratio ($r_b = \sigma_b/\sigma_s$) using the following relationships:

$$\sigma_m = \sigma_s - \sigma_b = (1 - r_b)\sigma_s \tag{2.2}$$

$$\sigma_b = r_b \sigma_s \tag{2.3}$$

Since σ_m and σ_b can be readily calculated using numerical implementation with either solid element or shell element as elaborated in [12], for any stress combination and crack depth, the corresponding SIF can be determined as long as the geometric correction factors Y_m and Y_b are known.

Utilizing a comprehensive set of numerical simulations with two-dimensional elements, Brennan et al. [22] provided expressions for Y_m and Y_b after conducting regression and optimization analysis (see Appendix A for complete expressions). It is insisted that the equations should be used only for the following ranges:

Range of crack depths: $0.01 \leq a/t \leq 1.0$

Range of crack aspect ratios: $0 \leq a/c \leq 1.0$

Range of weld angles: $30° \leq \alpha \leq 60°$

Range of attachment widths: $0.3 \leq L/t \leq 4.0$

Range of weld toe radii: $0.01 \leq \rho/t \leq 0.066$

The graphical illustration of the above terminologies can be seen in Fig. 2.1.

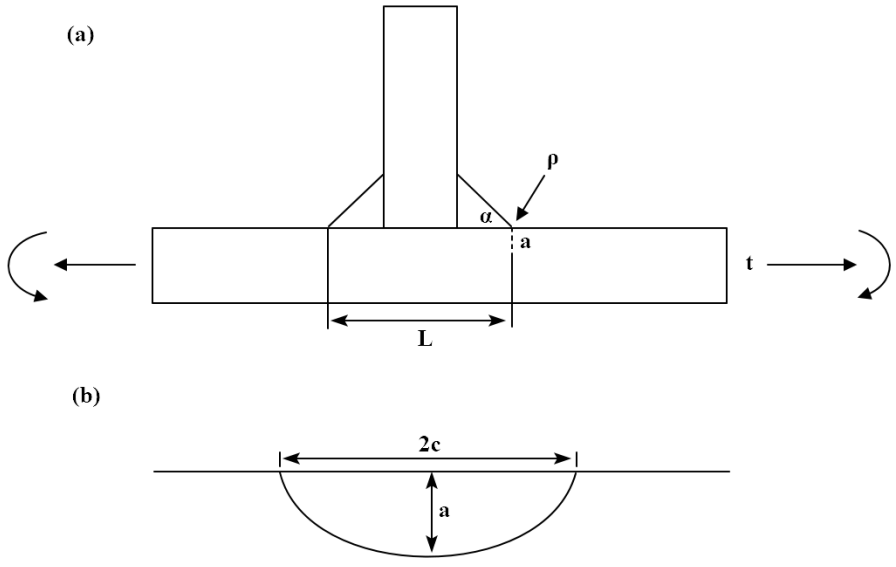

Fig. 2.1 (a) Weld geometry and loadings used to derive stress intensity factors; (b) crack geometry (semi-elliptical crack).

The above parametric equations developed by Brennan et al. are mainly intended and focused on the application to marine and offshore structures, which typically have a large plate thickness so that ρ/t is very small. As mentioned earlier, however, for many structures in the automotive and mechanical industries, welded thin sheets are used that form a large value of ρ/t. For example, the data measured in document [38] and the test data completed in this study both show that $\rho/t > 0.066$. It is unclear whether the above mentioned parametric equations can still work when the welded structures have a value of ρ/t out of the validity range. For this reason, a two-dimensional FEA simulation was carried out in this study with various weld toe radii, up to $\rho/t = 0.5$ for a T-butt weld joint. The stress distribution at the potential crack initiation site was extracted from the FEA result and then used as input into a weight function solution to determine the SIFs. Finally, the geometric correction factors were calculated from the obtained SIFs and compared with Brennan's parametric equations.

2.2 Niu-Glinka weight function

To validate Brennan's parametric equations, SIFs need to be determined for the cases of large weld toe radii. Here, the Niu-Glinka weight function method [19, 20] is used in combination with the stress output from FEA to calculate the SIFs by integrating the following expression:

$$K = \int_0^a \sigma(x) m\left(x, \frac{a}{t}, \frac{a}{c}, \alpha\right) dx \tag{2.4}$$

where $m\left(x, \frac{a}{t}, \frac{a}{c}, \alpha\right)$ is the weight function in terms of plate thickness t, crack depth a, crack aspect ratio $\frac{a}{c}$, and weld angle α and is documented in the literature [19], and $\sigma(x)$ is the normal stress distribution on the un-cracked cross-section at the critical point of the welded plate. Mode I failure is assumed to be the dominant failure mechanism at the weld toe.

2.3 FEA stress analysis

The normal stress distribution on the un-cracked plane is acquired by using two-dimensional FEA for a range of T-butt joint geometries (weld angle $\alpha = 30°, 45°$, and $60°$ and weld toe radius $\rho/t = 0.1, 0.3$, and 0.5). Here, the overall width of weld attachment L is taken as $2t$, based on current measurements that L/t is usually larger than 2, and it has been shown [22] that the Y_m and Y_b barely change when L is larger than $2t$. So, the results with the setting of $L = 2t$ can be approximately used for the cases where $L/t \geq 2$.

Second-order elements with fine meshes are used in order to get higher accuracy. Plane strain condition is used because the width of the joint is much larger than the thickness. A mesh convergence study has been done to make sure the number of elements is large enough to get a convergent stress result. The schematic diagram of the FEA model is shown in Fig. 2.2. Symmetric boundary conditions are applied to save computing time and effort given the fact that the geometry is symmetric with the vertical centerline of the attachment. Uniform stress field and linearly decreasing stress field are applied separately to the far end to simulate the conditions of pure tension and pure bending. A typical normal stress distribution at the critical cross-section under pure tension and pure bending, respectively, is given in Fig. 2.3, with the unit load applied.

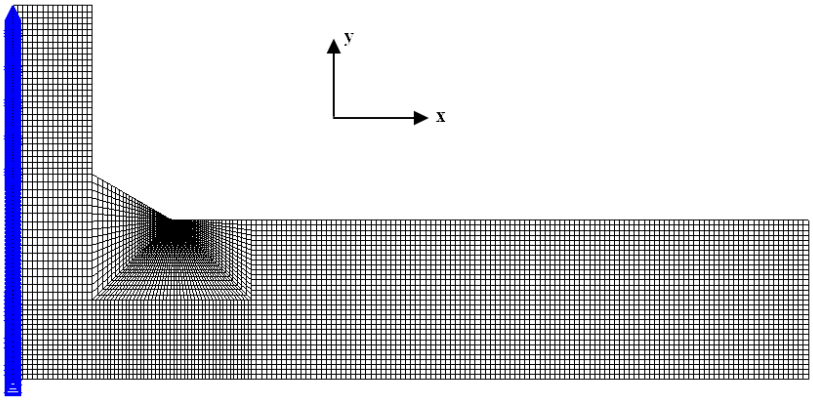

(a)

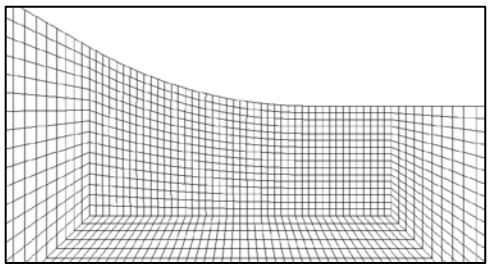

(b)

Fig. 2.2 Schematic diagram of (a) FEA model and (b) FEA model of the weld toe

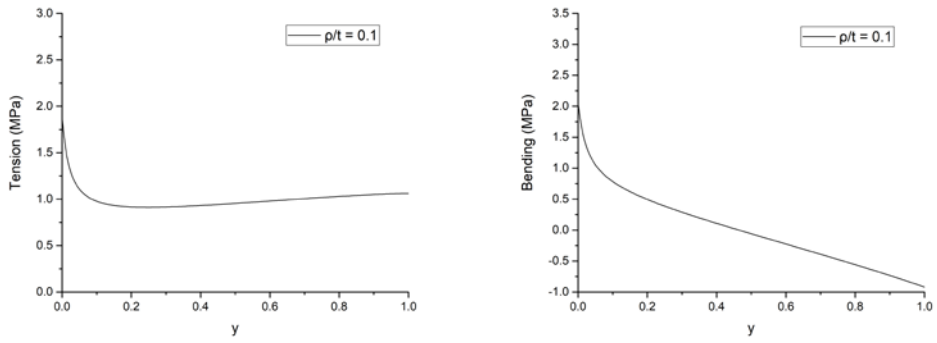

(a) (b)

Fig. 2.3 Normal stress distribution at the critical cross-section with unit load under (a) pure tension; (b) pure bending when $\alpha = 45°$ and $\rho/t = 0.1$

2.4 Validation of the parametric equations for SIFs calculation

After the normal stress distributions $\sigma(x)$ are extracted from the FEA stress analysis, they are used as inputs into Eq. (2.4) to determine the SIFs. The implementation of integration on Eq. (2.4) follows the efficient integration steps described in [39].

The parametric equations for SIFs given by Brennan et al. are expressed in the form of geometric correction factors Y_m and Y_b (they are equivalent to the SIFs). So, the values of Y_m and Y_b are used as the parameters to compare Brennan's equations and the FEA results. The comparisons are made for various weld angles and various weld toe radii, as seen in Figs. 2.4–2.9, and the crack aspect ratio a/c is taken from 0.2 to 1 because a semi-elliptical crack shape is assumed during the crack propagation period in this study.

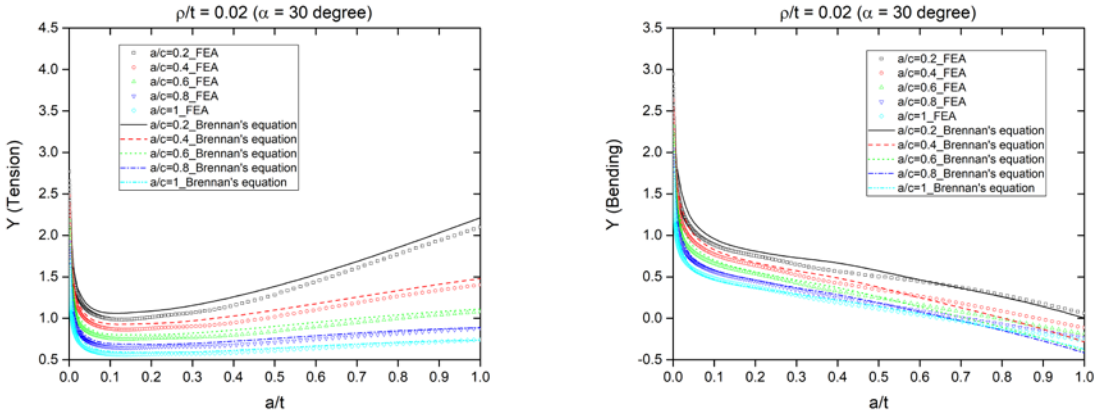

(a)

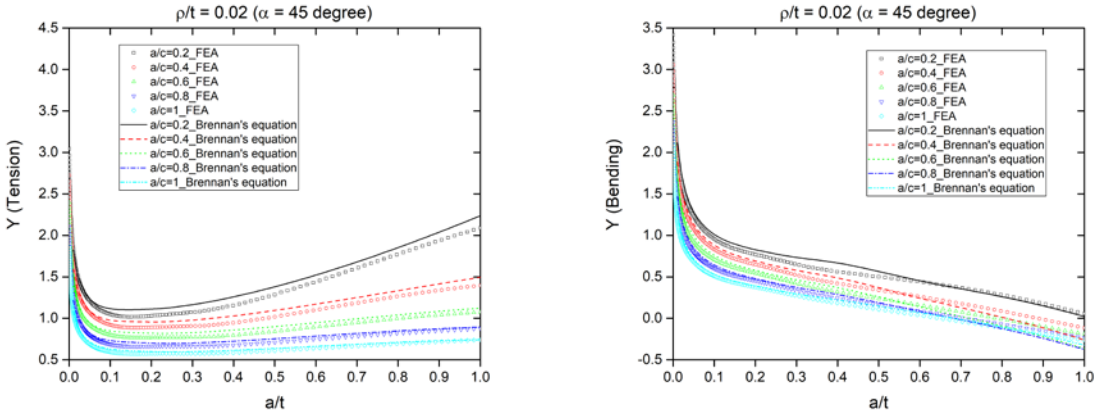

(b)

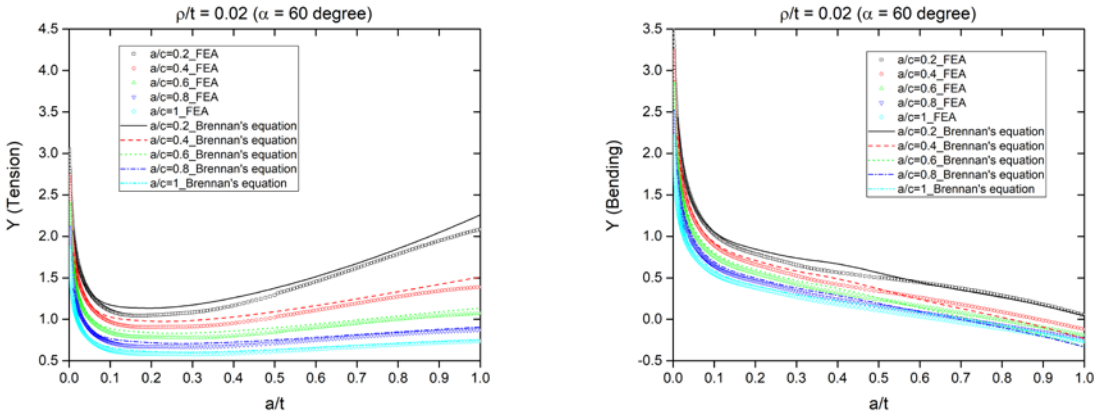

(c)

Fig. 2.4 Comparison of geometric correction factors Y_m and Y_b between Brennan's equations and FEA results for $\rho/t = 0.02$ and (a) $\alpha = 30°$, (b) $\alpha = 45°$, (c) $\alpha = 60°$

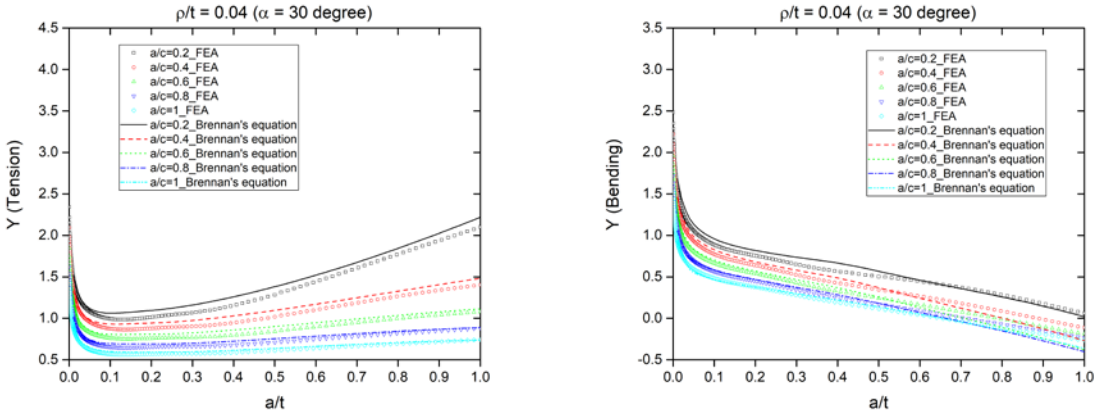

(a)

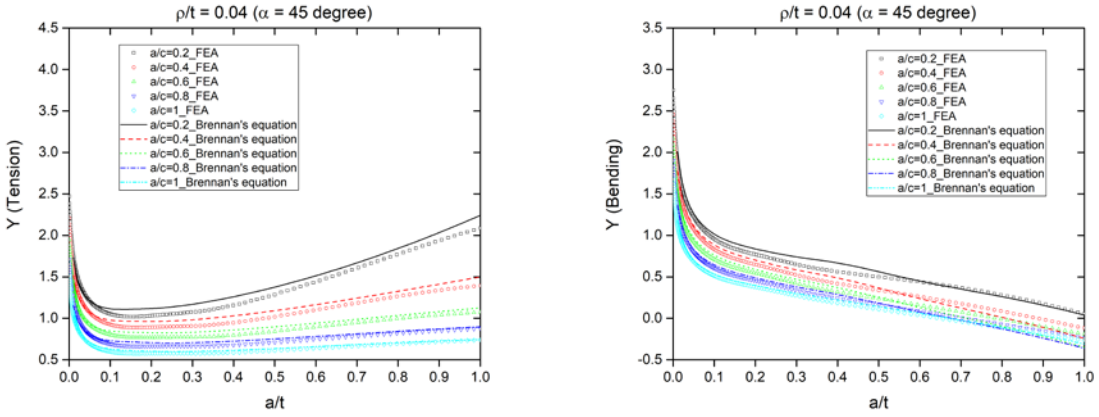

(b)

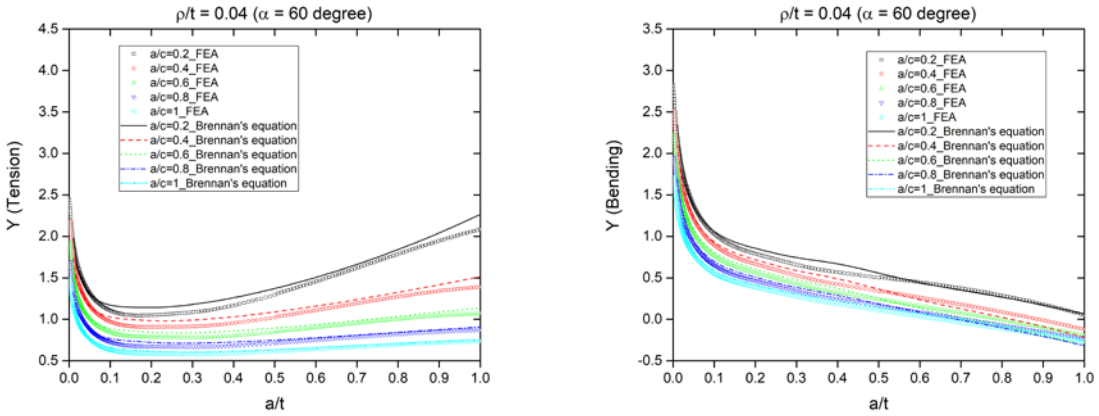

(c)

Fig. 2.5 Comparison of geometric correction factors Y_m and Y_b between Brennan's equations and FEA results for $\rho/t = 0.04$ and (a) $\alpha = 30°$, (b) $\alpha = 45°$, (c) $\alpha = 60°$

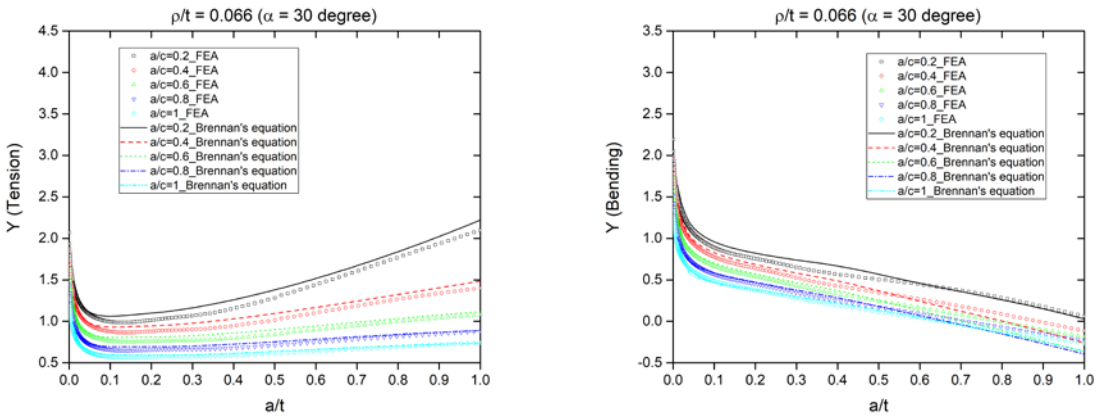

(a)

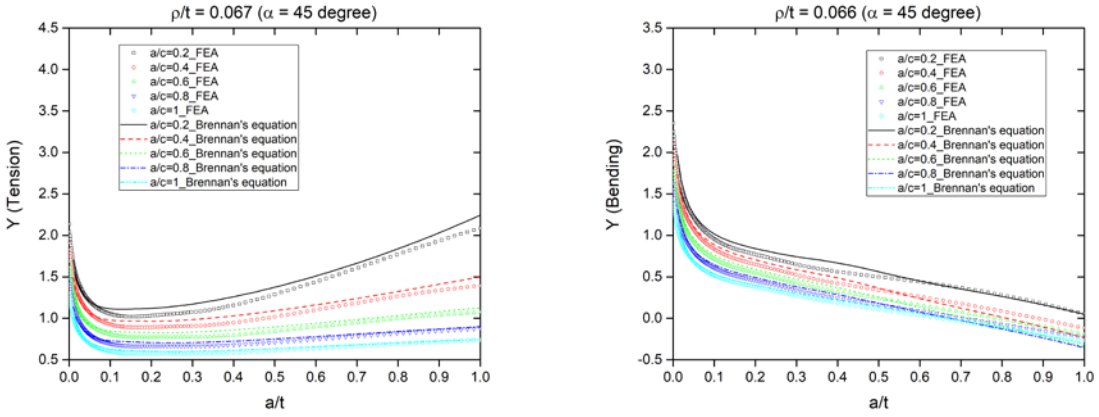

(b)

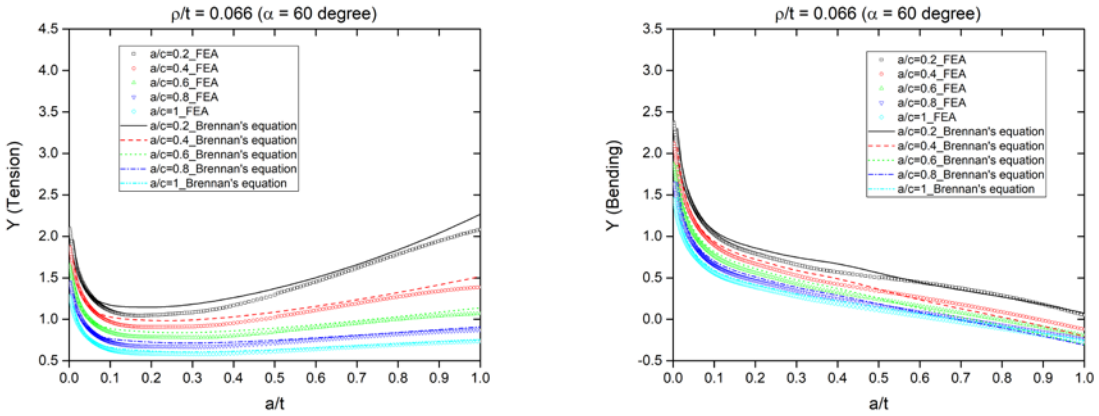

(c)

Fig. 2.6 Comparison of geometric correction factors Y_m and Y_b between Brennan's equations and FEA results for $\rho/t = 0.066$ and (a) $\alpha = 30°$, (b) $\alpha = 45°$, (c) $\alpha = 60°$

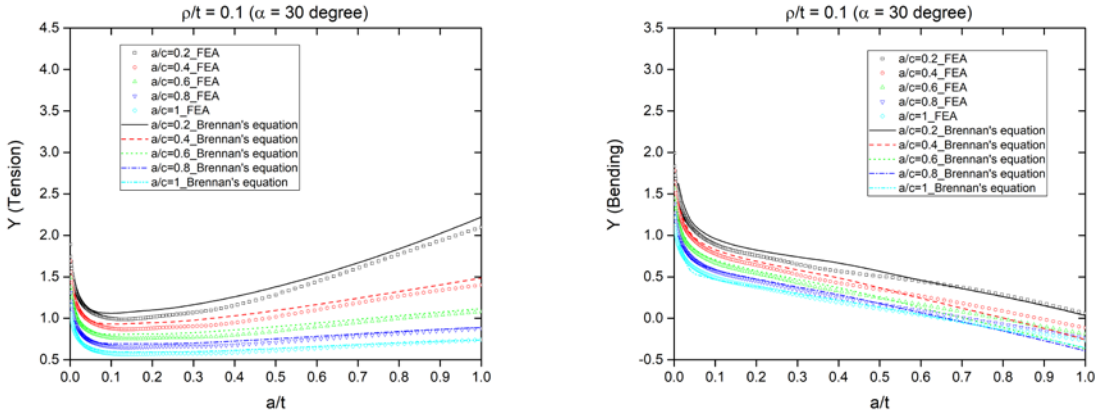

(a)

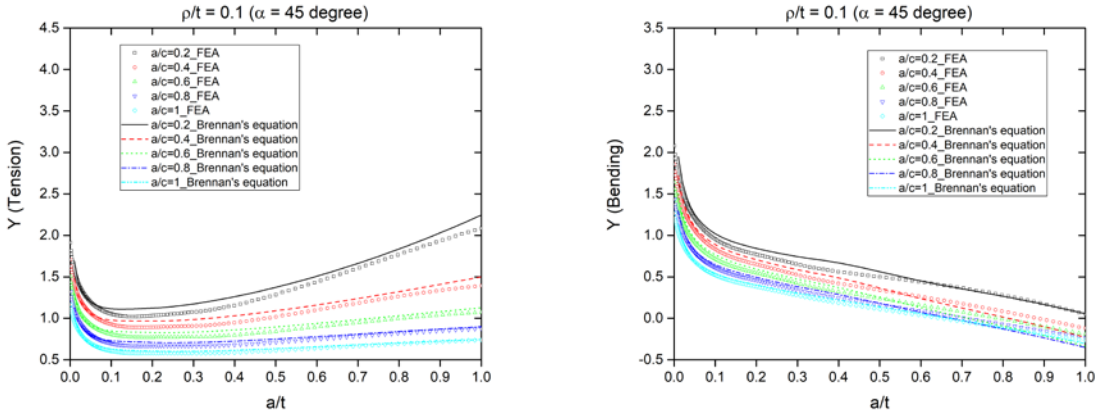

(b)

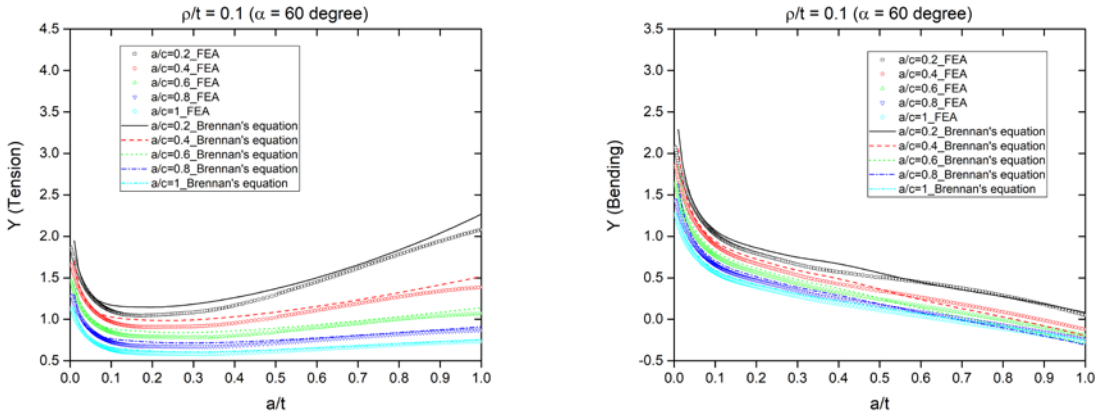

(c)

Fig. 2.7 Comparison of geometric correction factors Y_m and Y_b between Brennan's equations and FEA results for $\rho/t = 0.1$ and (a) $\alpha = 30°$, (b) $\alpha = 45°$, (c) $\alpha = 60°$

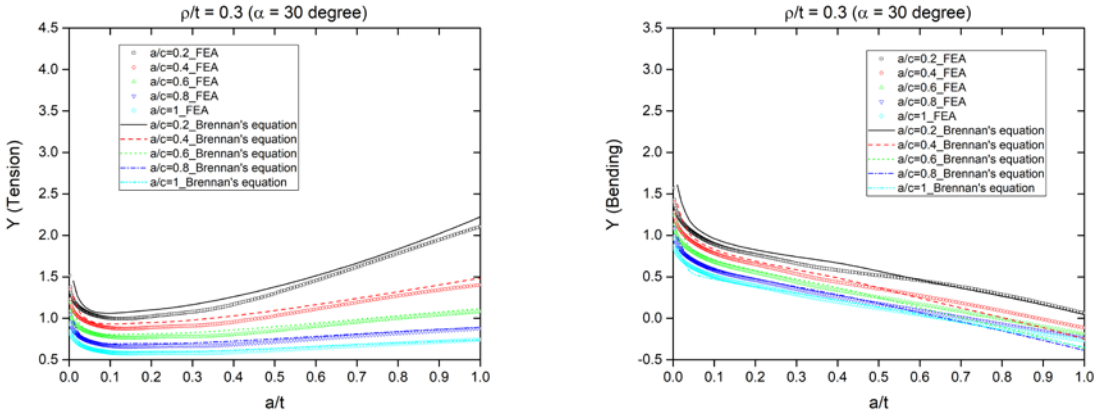

(a)

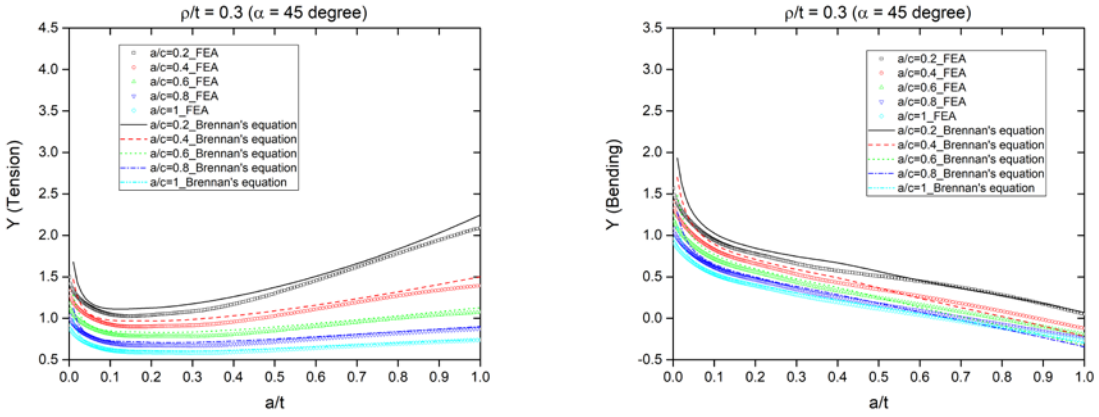

(b)

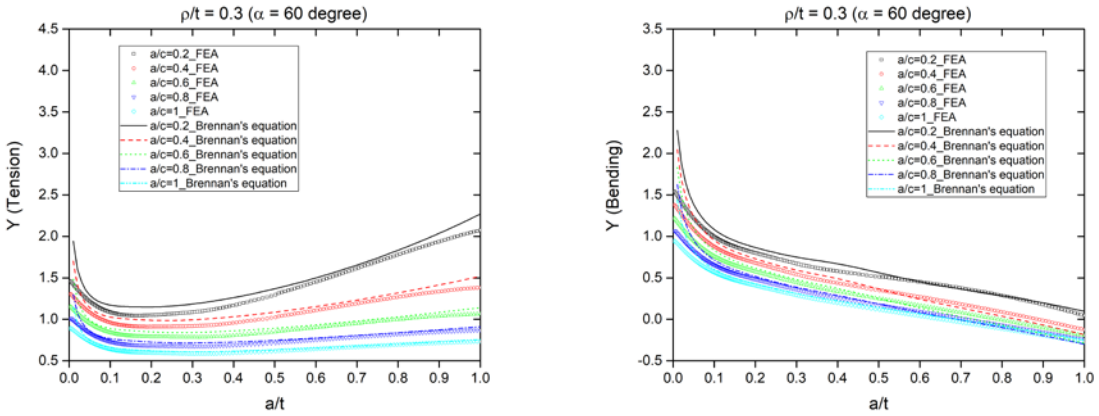

(c)

Fig. 2.8 Comparison of geometric correction factors Y_m and Y_b between Brennan's equations and FEA results for $\rho/t = 0.3$ and (a) $\alpha = 30°$, (b) $\alpha = 45°$, (c) $\alpha = 60°$

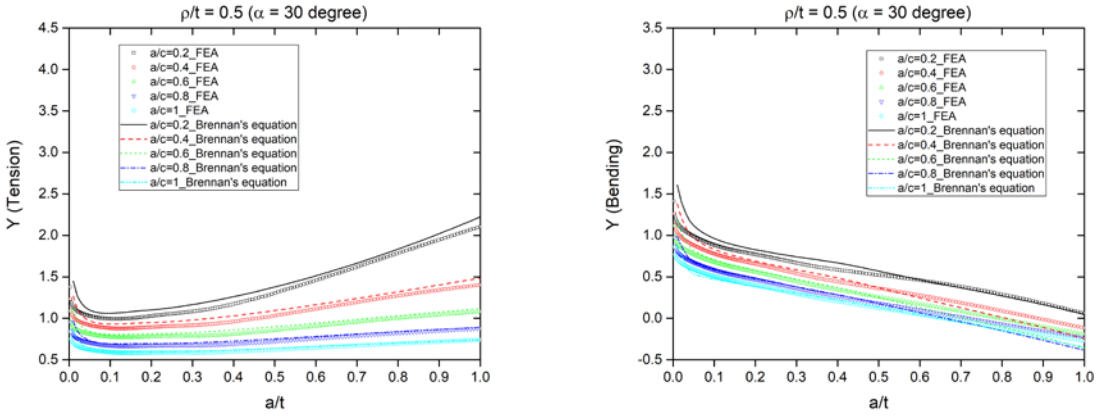

(a)

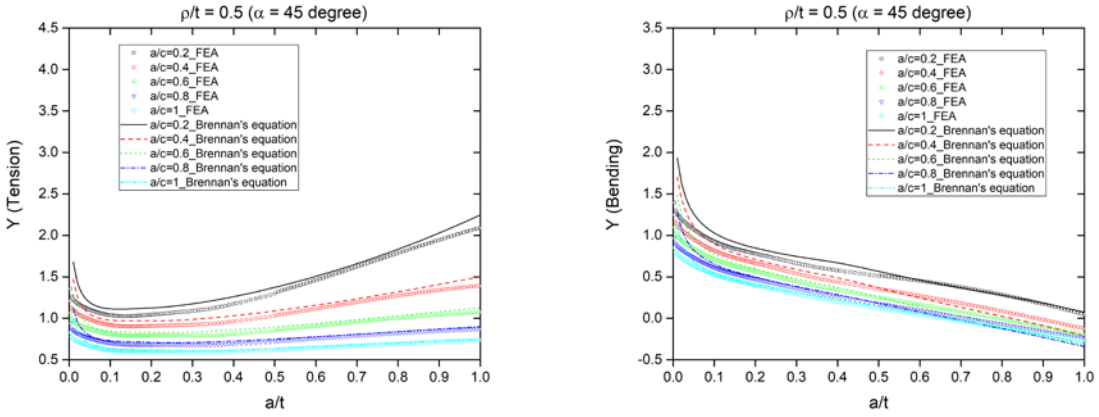

(b)

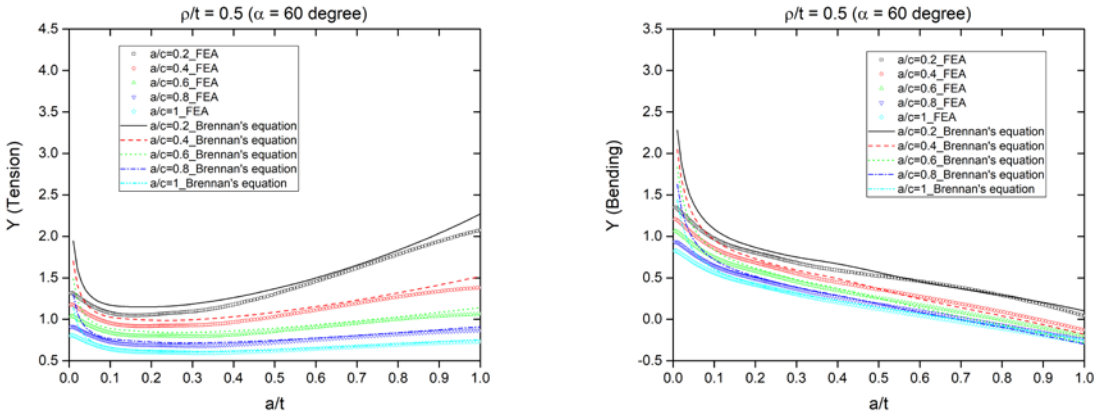

(c)

Fig. 2.9 Comparison of geometric correction factors Y_m and Y_b between Brennan's equations and FEA results for $\rho/t = 0.5$ and (a) $\alpha = 30°$, (b) $\alpha = 45°$, (c) $\alpha = 60°$

As can be seen in Figs. 2.4–2.9, the geometric correction factors Y_m and Y_b change along the crack depth a/t, and the behaviors of Y_m and Y_b are different. The weld angle α , the weld toe radius ρ/t, and the crack aspect ratio a/c affect on the distributions of Y_m and Y_b. For the cases of $\rho/t \leq 0.1$, Brennan's equations coincide very well with the FEA results under either tensile loading or bending loading for any weld angle and any crack aspect ratio. For the cases of $\rho/t = 0.3$ and $\rho/t = 0.5$, small differences between Brennan's equations and FEA results occur in the short crack region (a/t up to 0.05), especially for the large weld angles ($\alpha = 45°$ and $\alpha = 60°$). Though small differences exist, the majority of the ranges of Y_m and Y_b from FEA are well described by the parametric equations. The small differences are partly caused by the intrinsic error during the regression process of the parametric equations and the calculation error induced in the integration of the weight functions. Meanwhile, the differences show that Brennan's equations slightly overestimated the FEA results in the short crack region. This means that if the equations are used, they will provide, to some extent, shorter (conservative) estimated fatigue life, which is actually preferable in engineering applications. Therefore, based on these facts, it is believed by the authors that the effects of the weld angle and weld toe radius on the SIFs are satisfactorily captured by the Brennan's parametric equations and they can still be used to calculate the SIFs for large weld toe radii cases (ρ/t up to 0.5).

CHAPTER III

GENERALIZED STRESS PARAMETER APPROACH

3.1 Derivation

In the fracture mechanics field, Paris' Law [16] provides a simple mathematical relationship between the crack growth rate (da/dN) and the range of the stress intensity factor, ΔK, when cyclic loading is applied. In its simplest form, it is expressed as

$$\frac{da}{dN} = C(\Delta K)^m \tag{3.1}$$

where C and m are material constants.

Thus, the fatigue life can be estimated by integrating Eq. (3.1):

$$N = \int \frac{1}{C(\Delta K)^m}\, da = \frac{1}{C} \cdot t^{1-\frac{m}{2}} \cdot (\Delta\sigma_s)^{-m} \cdot \int \frac{1}{\left(\sqrt{\frac{\pi a}{t}}[Y_m(1-r_b)+Y_b r_b]\right)^m}\, d\left(\frac{a}{t}\right)$$

$$= \frac{1}{C} \cdot t^{1-\frac{m}{2}} \cdot (\Delta\sigma_s)^{-m} \cdot I(Y_m, Y_b, r_b) \tag{3.2}$$

Here, $I(Y_m, Y_b, r_b) = \int \frac{1}{\left(\sqrt{\frac{\pi a}{t}}[Y_m(1-r_b)+Y_b r_b]\right)^m}\, d\left(\frac{a}{t}\right)$ is the crack propagation integral and has a dimensionless form. As has been shown in the previous section, Brennan's parametric equations for Y_m and Y_b can be used for a wide spectrum of welded geometries without losing accuracy; thus, the term $I(Y_m, Y_b, r_b)$ becomes a function of weld angle α, weld toe radius $\frac{t}{\rho}$, crack aspect ratio $\frac{a}{c}$, and bending ratio r_b.

Furthermore, by organizing the stress term to the left-hand side, Eq. (3.2) can be rewritten as:

$$\Delta\sigma_s = C^{-\frac{1}{m}} \cdot t^{\frac{2-m}{2m}} \cdot I(Y_m, Y_b, r_b)^{\frac{1}{m}} \cdot N^{-\frac{1}{m}} \tag{3.3}$$

From Eq. (3.3), Maddox [23] defined a so-called "generalized stress parameter" as:

$$\Delta S = \frac{t^{\frac{m-2}{2m}}}{I(Y_m, Y_b, r_b)^{\frac{1}{m}}} \Delta\sigma_s \tag{3.4}$$

In Eq. (3.4), $\Delta\sigma_s$ is the structural stress range, which captures the stress concentration effect caused by the global structural geometry. The term $t^{\frac{m-2}{2m}}$ can be seen as a thickness correction for the cases of $t \neq 1$, in order to compensate for the effect induced by different thicknesses for various welded components or structures. It turns to unity when $t = 1$; therefore, t can be alternatively interpreted as the ratio of the actual thickness to a unit thickness. With this interpretation, $t^{\frac{m-2}{2m}}$ becomes dimensionless and ΔS remains a stress unit. As mentioned earlier, the dimensionless integral term $I(Y_m, Y_b, r_b)^{\frac{1}{m}}$ is related to the local weld geometries (such as weld angle and weld toe radius, etc.), which takes the local stress concentration effect caused by the weld profile into consideration, and bending ratio r_b, which concerns the loading mode effect.

The generalized stress parameter ΔS constitutes a new fatigue damage parameter that includes the local weld profile effect compared to the structural stress parameter. Identical to the traditional S-N curve method, the generalized stress parameter has a logarithmic linear relationship with the fatigue life, shown as

$$\Delta S = C' N^b \tag{3.5}$$

where C' is the fatigue strength coefficient and b is the fatigue strength exponent.

It is necessary to have an expression for $I(Y_m, Y_b, r_b)^{\frac{1}{m}}$ in order to calculate the generalized stress parameter ΔS. Based on the definition of $I(Y_m, Y_b, r_b)^{\frac{1}{m}}$, numerical integrations are carried out by using the multivariate regression method, and a simple parametric expression is obtained as

$$I(Y_m, Y_b, r_b)^{\frac{1}{m}} = 2.325 + 0.426 * e^{0.350\alpha} * \left(\frac{\rho}{t}\right)^{-0.020+0.007\alpha} * (e^{(-9.783+9.704r_b)} + 0.164r_b - 1.833) \quad (3.6)$$

Here, the crack aspect ratio a/c is assumed to be 0.25 based on the experimental observations, and the fatigue crack growth factor m is taken as 3.6 for steel according to published crack growth data.

Fig. 3.1 shows the comparison of the fitted Eq. (3.6) and the calculated data points for $I(Y_m, Y_b, r_b)^{\frac{1}{m}}$. The weld angle α ranges from 30° to 60°, and the weld toe radius $\frac{\rho}{t}$ varies between 0.02 and 0.5. These values are chosen as an attempt to cover most of the measured weld data on hand. It should be noted that when carrying out the integral calculation for $I(Y_m, Y_b, r_b)^{\frac{1}{m}}$, without knowing the initial crack depth a_i, it is assumed that $a_i/t = 0.01$ here since it is the smallest effective value in the validity range of Brennan's equations. Additionally, the relative final crack depth $a_f/t = 0.8$ is adopted in the integral process as a result of observations on the tested data. As shown in Fig. 3.1, the distribution and trend of $I(Y_m, Y_b, r_b)^{\frac{1}{m}}$ are well captured by Eq. (3.6).

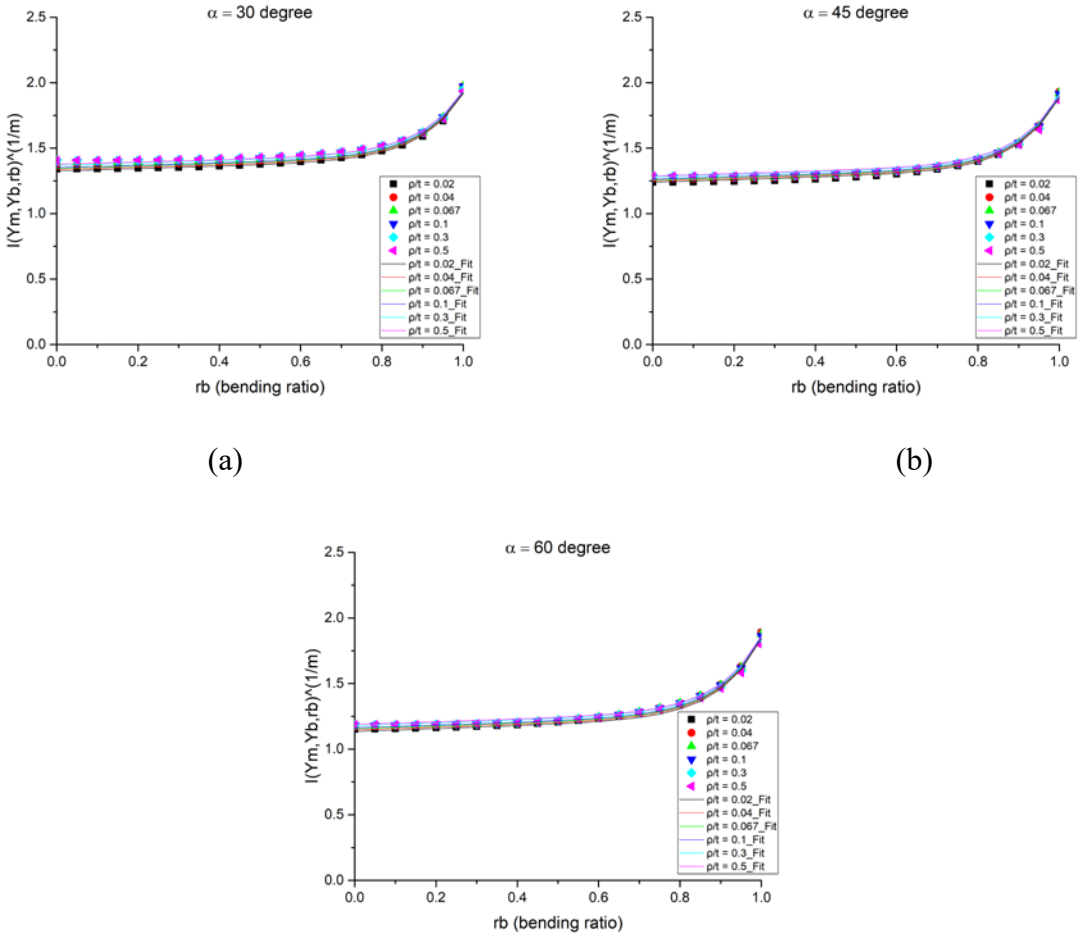

Fig. 3.1 Comparison of Eq. (3.6) and integrated data points for $I(Y_m, Y_b, r_b)^{\frac{1}{m}}$ with (a) $\alpha = 30°$, (b) $\alpha = 45°$, and (c) $\alpha = 60°$

3.2 Mean stress correction

In the fatigue analysis, the mean stress may have an effect on the fatigue strength of the material or joints. Fig. 3.2 shows a typical cyclic loading case, on which σ_{max} represents the maximum stress and σ_{min} means the minimum stress. The difference between maximum stress and minimum stress is called the stress range, $\Delta\sigma$. The stress amplitude σ_a is half of the stress

range $\Delta\sigma$. A stress ratio, R is defined as the ratio of minimum stress to maximum stress to characterize the mean stress effect in fatigue analysis:

$$R = \frac{\sigma_{min}}{\sigma_{max}} \tag{3.7}$$

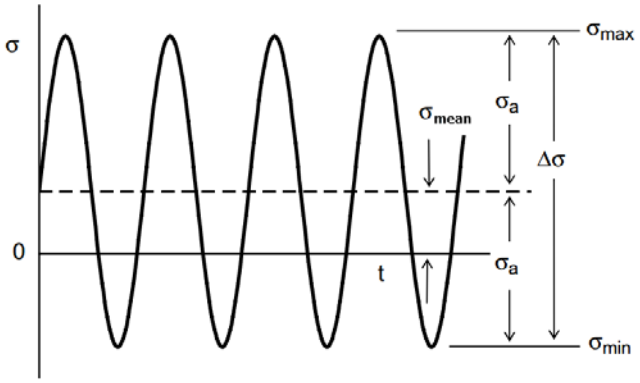

Fig. 3.2 Definitions of cyclic loading

The mean stress effects have long been studied [40-42]. Among them, the Smith, Watson, and Topper (SWT) equation is one of the most commonly used in assessing the mean stress effects for component life data. The SWT equation for stress-life fatigue is expressed as:

$$\sigma_{ar} = \sqrt{\sigma_{max} * \sigma_a} \tag{3.8}$$

where σ_{ar} is the fully reversed stress amplitude.

Eq. (3.8) means that a given loading case with a mean stress can be transformed into an equivalent loading case which has zero mean stress. By using the terminologies defined in the beginning, Eq. (3.8) can be rewritten in terms of stress range:

$$\Delta\sigma_r = \sqrt{\frac{2}{1-R}}\Delta\sigma_s \tag{3.9}$$

where $\Delta\sigma_r$ is the fully reversed structural stress range.

Substituting Eq. (3.9) into Eq. (3.4) will lead to the GSP equation with mean stress corrections:

$$\Delta S = \frac{\left(\frac{2}{1-R}\right)^{\frac{1}{2}}}{t^{\frac{2-m}{2m}} * I(Y_m, Y_b, r_b)^{\frac{1}{m}}} \Delta\sigma_s \tag{3.10}$$

After the local weld profile is measured, the generalized stress parameter can be calculated using either Eq. (3.4) or Eq. (3.10), depending on whether mean stress effects need to be considered or not. The following part will show and discuss the capability of the generalized stress parameter to correlate the fatigue data for different types of welded joints with various local geometries under different loading modes.

CHAPTER IV

VALIDATION WITH FATIGUE TEST RESULTS

4.1 Fatigue test and results

To validate the method proposed in this study, more than 400 fatigue tests for several different types of welded joints were conducted, and the results were collected. The gas metal arc welding (GMAW) technique was utilized to weld the separate steel sheets together to fabricate the specimens. The samples tested in this study are butt welded joint, lap welded joint, and fillet welded joint, and their dimensions are shown in Fig. 4.1. The specimens were provided by Auto/Steel Partnership and they have the same geometries as those used in previous investigations [38]. Six different thickness combinations were used. Table 1 summarizes the joint types and their thickness combinations tested in this study.

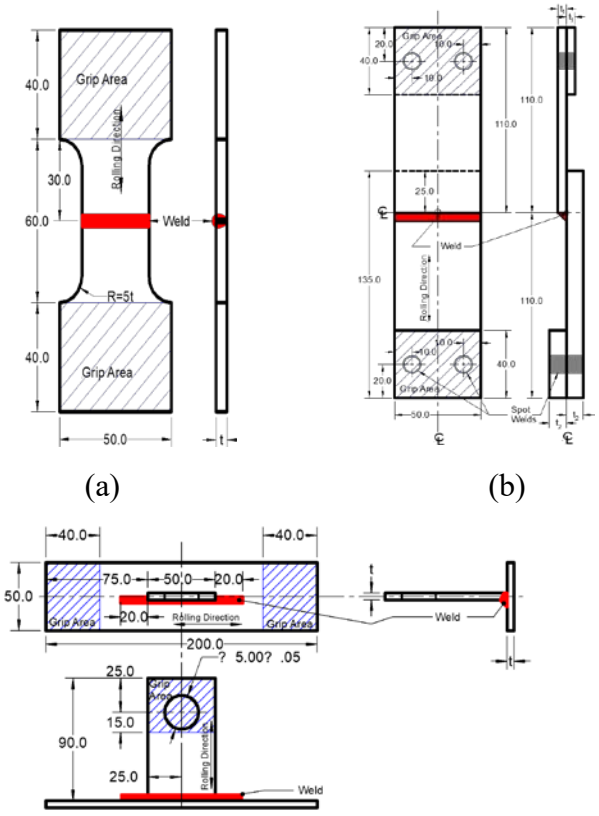

Fig. 4.1 Geometries and dimensions of (a) butt welded joint, (b) lap welded joint, and (c) fillet welded joint

Table 4.1 Joint types and thickness combinations

Joint types	Thickness combinations					
Butt joint	1mm-1mm	2mm-2mm	1mm-2mm	1.4mm-1.4mm	-	-
Lap joint	1mm-1mm	2mm-2mm	1mm-2mm	1.4mm-1.4mm	2.5mm-2.5mm	1.4mm-2.5mm
Fillet joint	1mm-1mm	2mm-2mm	1mm-2mm	1.4mm-1.4mm	2.5mm-2.5mm	-

The base material is made of advanced high strength steel (AHSS). Three different steel grades are tested, i.e., Dual Phase 780, Dual Phase 980 and Complex Phase 800. Note that it is reported in [38] that the parent metal strength does not affect the fatigue strength of GMAW, and similar conclusions are found in this study. So the effect of the parent material is not considered

in this thesis. Load control fatigue with two loading ratios R=0.1 and R=0.3 are tested with various load ranges. It is also found both in [38] and in this study that the loading ratio has a negligible effect on the fatigue life of the tested welded joints, so it is not considered in this work.

Fig. 4.2 shows the fatigue load range vs. fatigue life data for the tested joints. The data points that have a fatigue life lower than 1000 are not included since plastic deformation usually will occur in low-cycle regimes with high cyclic loadings. The fatigue behavior in this region may be different and can be corrected by the methods introduced in [43]. Run-out data are also not plotted.

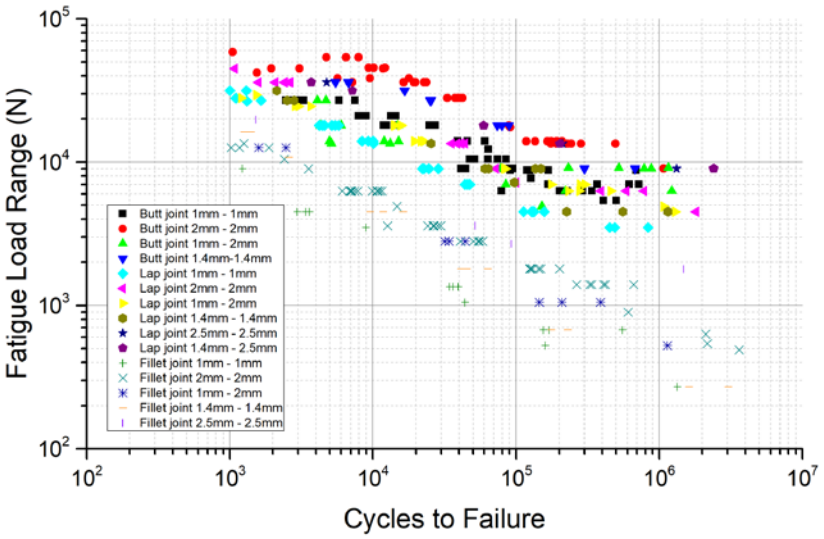

Fig. 4.2 Fatigue load range vs. cycles to failure for different specimen types and thicknesses

As can be seen in Fig. 4.2, for a given fatigue load range, the fatigue life between different joint types can vary significantly. It means the fatigue strength is strongly dependent on the joint type. Meanwhile, as expected, the thicker specimen has a longer fatigue life comparing to the thinner one. These effects are not considered in the fatigue load range vs. life curves. A fatigue

damage parameter is deemed to be good and promising, only if most of the distributed data points can collapse into a narrow band when using it for fatigue assessment.

4.2 FEA modeling with shell elements

To evaluate the proposed generalized stress parameter method, and compare it with currently widely used structural stress methods, 3-D FEA models are built with shell elements for each joint type, as shown in Fig. 4.3. These coarsely meshed models are established using HyperMesh based on the meshing guidelines in the nCode manual [26]. The linear elastic analysis is used with Young's Modulus set as 210 GPa and Poison's ratio as 0.3. Boundary conditions are applied following the testing configurations.

After setting up the loading conditions and imputing the required information, commercial FEA software OptiStruct is employed to run the analysis. Note that the purpose of this analysis is not to calculate the structural stress (they need to be calculated by using certain post-processing procedures/software) but to extract the nodal forces and nodal moments, which are the basis to obtain the structural stress results, as discussed in Chapter I.

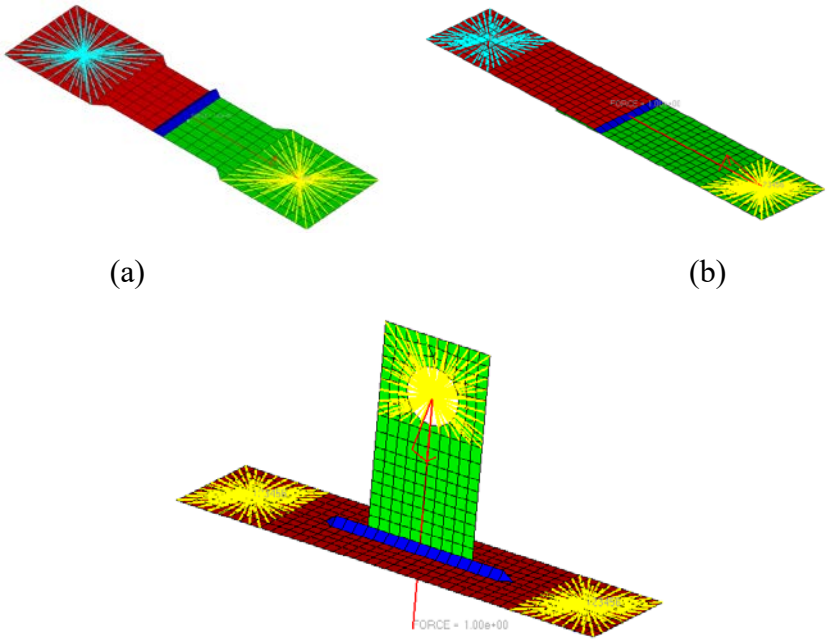

Fig. 4.3 Coarsely meshed models of (a) butt welded joint, (b) lap welded joint, and (c) fillet welded joint

4.3 Structural stress results

As introduced in Chapter I, the most famous structural stress methods, modified Fermer's approach and Dong's approach, are implemented in commercial software nCode and Fe-safe, respectively. So, these two software are used to calculate their structural stress results after the nodal forces/moments are extracted from OptiStruct.

With Fig. 4.4 showing the nCode structural stress range vs. fatigue life data, Fe-safe structural stress results are plotted in Fig. 4.5. As can be seen in Fig. 4.4 and Fig. 4.5, in contrary to the large scatter in fatigue load range vs. life curves, all the test data points from different joint types and different thicknesses are collapsing into a single band, and good correlations are found in both methods. This means both methods are able to correlate the fatigue data for the tested joint types and the tested thickness combinations. The S-N curves constructed from these fatigue test

results may be used to predict the fatigue lives for complex components or other joint types. The coefficient of correlation, R square, which is a criterion to evaluate the correlation results, is 0.813 in nCode and 0.7731 in Fe-safe.

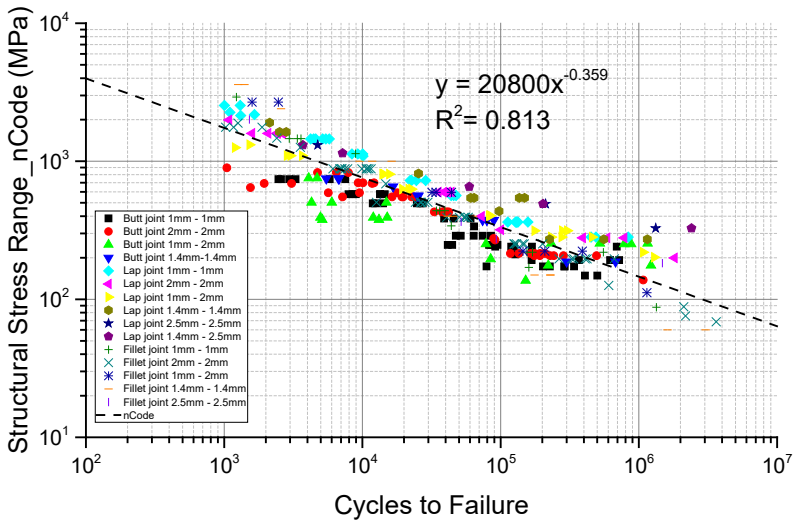

Fig. 4.4 nCode structural stress range vs. cycles to failure for different specimen types and thicknesses

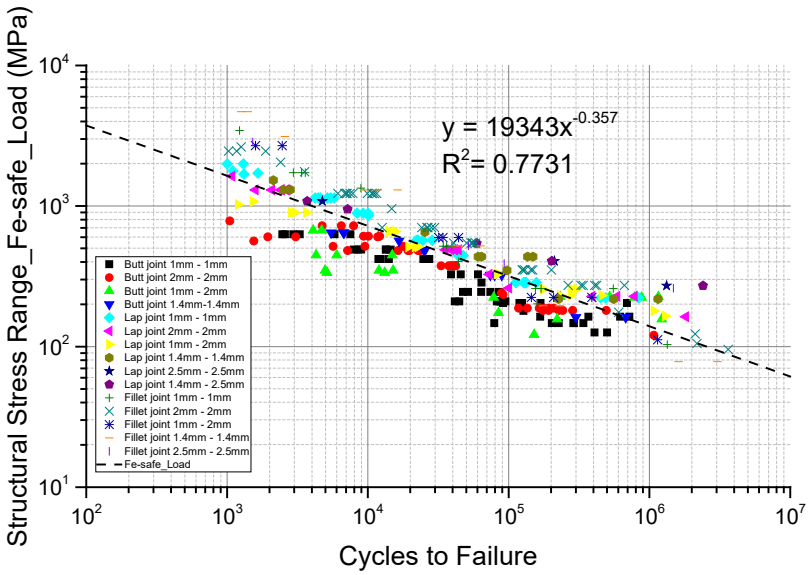

Fig. 4.5 Fe-safe structural stress range vs. cycles to failure for different specimen types and thicknesses

4.4 Measurements of weld dimensions

To calculate the generalized stress parameter from Eq. (3.4) and Eq. (3.6), the local dimensions of the welds are necessary. More specifically, the weld angle and weld toe radius must be measured for each specimen type and thickness combination based on the cross-section images. Figs. 4.6-4.8 shows examples of the cross-sections and the measurements for butt joint, lap joint and fillet joint.

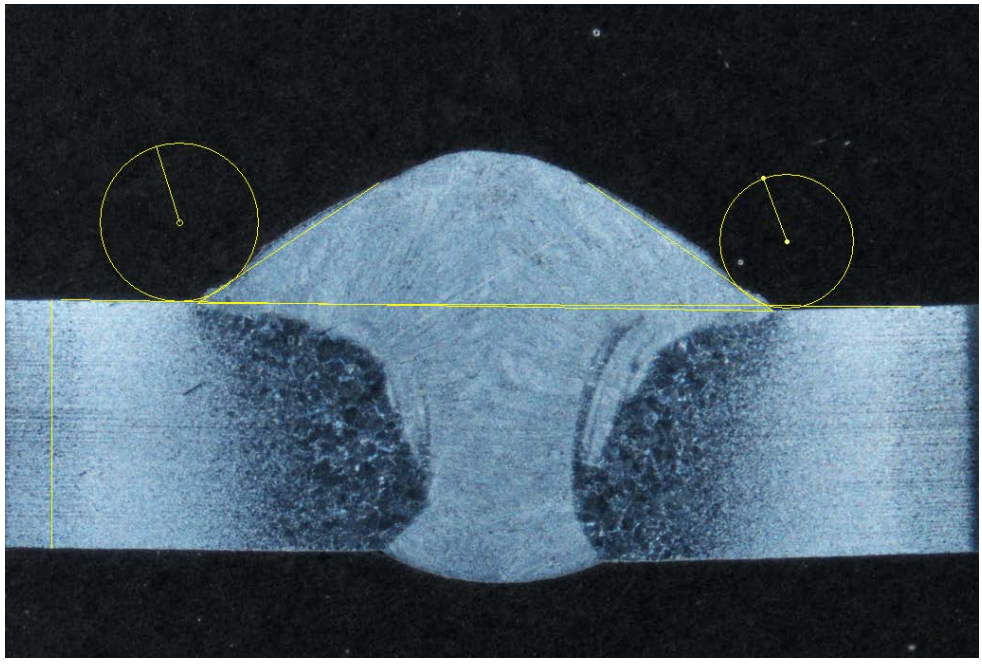

Fig. 4.6 Cross-section photo of the butt joint with 2mm thickness

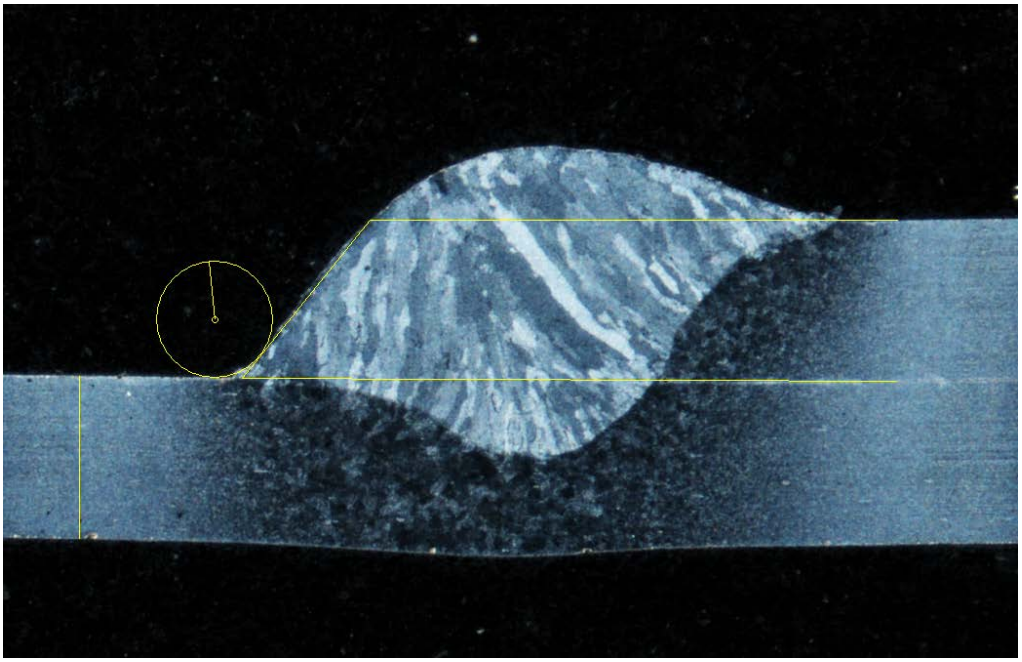

Fig. 4.7 Cross-section photo of the lap joint with 1mm thickness

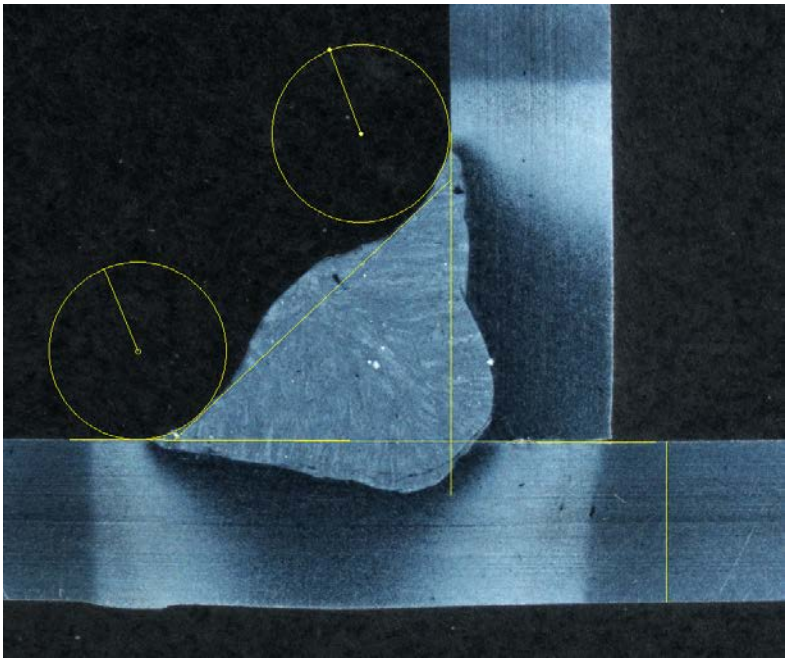

Fig. 4.8 Cross-section photo of the fillet joint with 2mm thickness

It is believed that the welding quality is very consistent, and two specimens are measured for each joint type with equal thickness while only one sample is measured for those with unequal

thicknesses to save cost. All the dimensions are recorded, and the average value is summarized in Table 4.2.

Table 4.2 Weld angle and weld toe radius data of butt joint

	Butt joint			
Thickness	1mm-1mm	2mm-2mm	1mm-2mm	1.4mm-1.4mm
Weld angle (degree)	49.878	42.641	59.441	31.209
Toe radius (mm)	0.138	0.362	0.156	0.289

Table 4.3 Weld angle and weld toe radius data of lap joint

	Lap joint					
Thickness	1mm-1mm	2mm-2mm	1mm-2mm	1.4mm-1.4mm	2.5mm-2.5mm	1.4mm-2.5mm
Weld angle (degree)	48.822	48.880	42.548	47.270	47.909	45.254
Toe radius (mm)	0.5045	1.1395	1.2510	0.718	1.118	1.589

Table 4.4 Weld angle and weld toe radius data of fillet joint

	Fillet joint				
Thickness	1mm-1mm	2mm-2mm	1mm-2mm	1.4mm-1.4mm	2.5mm-2.5mm
Weld angle (degree)	50.776	40.971	44.500	48.427	46.686
Toe radius (mm)	0.854	1.1445	0.507	1.336	0.490

4.5 Generalized stress parameter results

After the structural stress results are obtained, and the local dimensions are measured, the generalized stress parameter can be calculated straightforwardly using Eq. (3.6). Fig. 4.9 plots the generalized stress parameter range vs. fatigue life results. As can be seen, the scatter is reduced in comparison to the nCode and Fe-safe structural stress methods, and the coefficient of correlation

is increased to 0.8326. The reason for a higher correlation coefficient with the proposed Eq. (3.6) is that the generalized stress parameter not only considers the global geometric effect of the weldments, which is also accounted for by the structural stress, but also takes the local geometric effect into consideration. The explicit consideration of the local geometries, i.e., the weld angle α and the weld toe radius $\frac{\rho}{t}$, is reflected in the corresponding terms of the crack propagation integral $I(Y_m, Y_b, r_b)^{\frac{1}{m}}$. The improved correlation of fatigue data using the generalized stress parameter shows its ability to serve as a better fatigue damage parameter than the structural stress, based on current analyzed results.

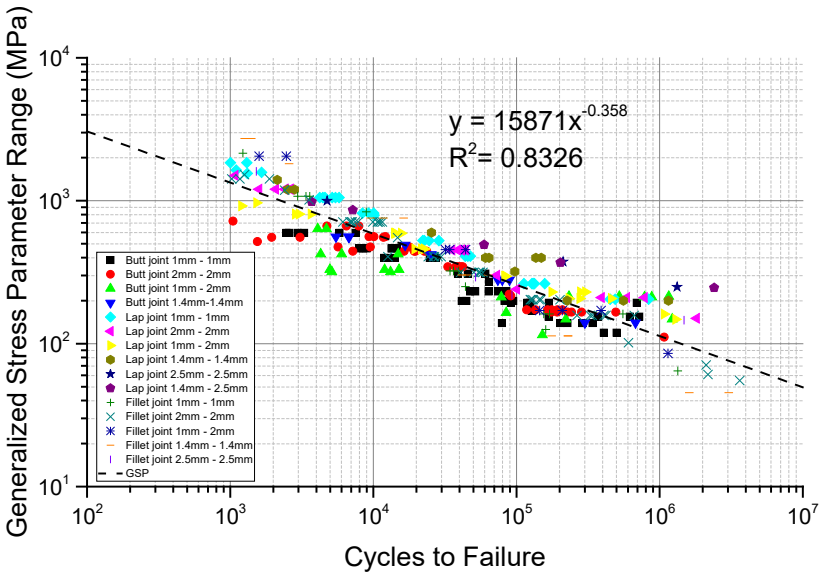

Fig. 4.9 Generalized stress parameter range vs. cycles to failure for different specimen types and thicknesses

4.6 Fatigue life estimation for thicker specimens

To further validate the proposed procedure to calculate the generalized stress parameter, two sets of lap welded joints and fillet welded joints with a greater thickness (4.9mm) are later tested, and the tested life is compared with the predicted fatigue life using the proposed model.

The parent material used for validation is hot rolled pickled and oiled (HRPO) steel. As mentioned earlier, however, the fatigue strength does not depend on the parent material.

The predicted life vs. tested life results for thicker specimens are plotted in Fig. 4.10. Along with the mean prediction line, a 95% confidence interval is given by the dashed lines, which is obtained from the regression result of the experimental database. As can be seen in Fig. 4.10, all of the experimental data for weld toe failure are located in the 95% prediction interval, with only one data point falling out of it. It means that the tested life is well predicted by the proposed generalized stress parameter method. Additionally, the majority of the data are under the mean prediction line, resulting in an underestimation of the tested life. This conservative result is usually favored for life prediction purposes. The capability to use the proposed GSP method is thus validated using these thicker specimens.

It should be noted that different failure modes can be observed during the testing procedure. For lap joints, two failure modes are found during the testing process, namely, weld toe failure and weld root failure. As for fillet joints, the majority display weld toe failure while a few show a mixed failure mode, in which it was difficult to distinguish whether they belong to toe failure mode or root failure mode. However, the failed specimens possess quite similar fatigue behavior (i.e. fatigue life) between these two failure modes. Thus, the approach proposed in this thesis, which is developed with a focus on the weld toe failure, can be used for the life prediction for both failure modes.

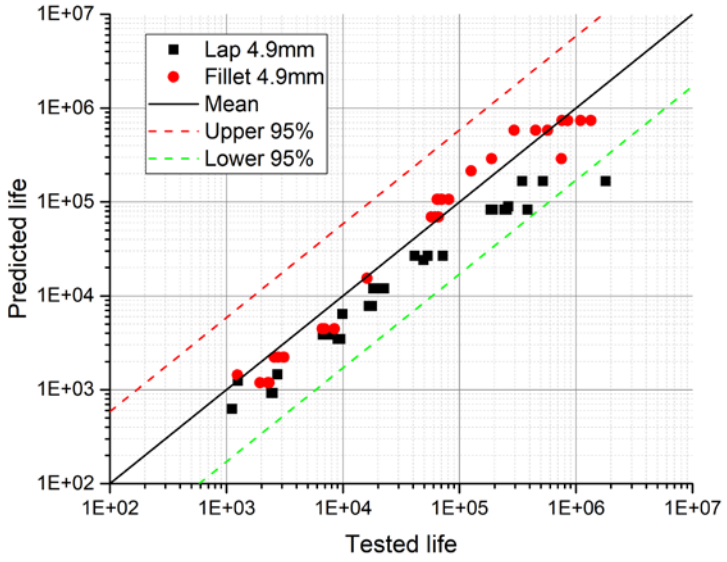

Fig. 4.10 Predicted life versus tested life for thicker specimens

4.7 Comparison with equivalent structural stress method

The author feels that it is necessary to have a clear comparison between the proposed generalized stress parameter (GSP) method and the equivalent structural stress (ESS) method because these two approaches share some similarities and differences.

It can easily be seen by comparing to Eq. (1.23) and Eq. (3.4), the equations to calculate the GSP and the ESS have the same structure. It is because they both come from the form proposed by Maddox [23]. While these two methods may share the same origin, some significant differences exist in many ways. Table 4.5 summarizes the main differences.

Table 4.5 Differences between GSP method and ESS method

Differences	GSP	ESS
Paris' Law	Original form $(\frac{da}{dN} = C(\Delta K)^m)$	Two-stage model $(\frac{da}{dN} = C(M_{kn})^n(\Delta K)^m)$
SIF calculation	Brennan's parametric equations	Magnification factor M_{kn}
Crack shape assumption	Semi-elliptical (a/c=0.25)	Semi-elliptical (a/c=0.6 for displacement control; a/c=0.2 for load control)
Weld local geometric effect	Explicitly considered (parameters α and $\frac{\rho}{t}$ are presented in $I(Y_m, Y_b, r_b)$)	Implicitly considered (But no dimension parameter is presented in $I(r)$)

The most important difference is, as discussed earlier that the GSP method can explicitly take the local geometric effect into consideration, which is reflected by including the local geometric dimensions in the term $I(Y_m, Y_b, r_b)$, and it is implicitly considered or only partially considered in ESS method.

CHAPTER V

CONCLUSIONS

In this thesis, two of the most popular and useful methods, structural stress method and fracture mechanics method, are reviewed in the first place. The structural stress methods are believed to be mesh-insensitive and are getting much attention nowadays. However, working as the nominal stress in welded joint, structural stress can only consider the global geometric effect, even though some corrections may be added in post-processing procedures. The stress intensity factor is the most important parameter used in the field of fracture mechanics and can consider the effect caused by the local geometries. The disadvantage is that its calculation is time-consuming.

This thesis presents a new approach to calculate a fatigue damage parameter called "generalized stress parameter (GSP)." The GSP concept is proposed on the foundation of fracture mechanics but remains in a close relationship with the structural stress method. This new approach provides the ability to consider the effect of local geometries, i.e., weld angle and weld toe radius (which are usually ignored in the classic structural stress method), so that it is very promising for fatigue life assessment. Major work and findings can be stated as follows:

(1) A number of two-dimensional FEA simulations are conducted to simulate the normal stress distribution for T-joints with various weld angles and different weld toe radii. Using the normal stress distribution as input, Niu-Glinka's weight function method is utilized to calculate the stress intensity factors (SIFs). The obtained SIF distributions

are then compared to Brennan's parametric equations, and it is found that the effectiveness of Brennan's equations still holds for large weld toe radius cases ($0.1 \leq \rho/t \leq 0.5$), which are common in automotive industry.

(2) The generalized stress parameter (GSP) is introduced and derived through the integration of Paris' Law. It is expressed in terms of the thickness correction term, the structural stress term, and the crack propagation integral. A parametric equation for the crack propagation integral, which explicitly includes the weld profile effect, is provided by regression of the calculated results. The regression results have shown that the proposed equation can capture its trend and distribution very well so that it can be formulated into the GSP calculation.

(3) A series of fatigue experiments have been performed on gas metal arc welded joints (GMAW) made of advanced high strength steel (AHSS). Three joint types are used with six different thickness combinations. The observation on the S-N curve results shows that, compared to the structural stress method, a better correlation is established using the GSP method, which considers the global and local geometric effect at the same time.

(4) For the validation purpose, additional fatigue tests are carried out using thicker welded specimens. The S-N curves constructed from previous results using the GSP method are used to predict the fatigue lives for the thicker specimens. The comparison results demonstrate that the test fatigue lives are well predicted using the GSP method, given that most of the validation data fall in the 95% prediction interval.

(5) Finally, discussions are made regarding the similarities and differences between GSP method and the equivalent structural stress (ESS) method. The comparison shows that

the GSP has the potential to serve as a better fatigue damage parameter than the structural stress or ESS, because of its extra capability in considering the local geometric effect.

APPENDIX

PARAMETRIC EQUATIONS FOR STRESS INTENSITY FACTORS

Tension

$$Y_m = 1.03\left(\frac{a}{t}\right)^P exp\left\{C_0 + C_1\left(\frac{a}{t}\right) + C_2\left(\frac{a}{t}\right)^2\right\} + C_3 + C_4$$

$$P = -0.365 + 0.207\left(\frac{a}{c}\right)^{0.5} - 0.144\left(\frac{a}{c}\right) + M_P$$

$$C_0 = -0.963 + 1.102\left(\frac{a}{c}\right)^{0.5} - 1.430\left(\frac{a}{c}\right) + M_0$$

$$C_1 = 3.084 - 6.542\left(\frac{a}{c}\right)^{0.5} + 9.023\left(\frac{a}{c}\right) + M_1 \quad \frac{a}{c} < 0.156$$

$$C_1 = 2.913 - 3.245\left(\frac{a}{c}\right)^{0.5} + 1.761\left(\frac{a}{c}\right) + M_1 \quad \frac{a}{c} \geq 0.156$$

$$C_2^1 = 2.627 - 10.767\left(\frac{a}{c}\right)^{0.5} + 9.553\left(\frac{a}{c}\right) \quad \frac{a}{c} < 0.2$$

$$C_2^1 = -0.0625 - 0.557\left(\frac{a}{c}\right)^{0.5} + 0.156\left(\frac{a}{c}\right) \quad \frac{a}{c} \geq 0.2$$

If $C_2^1 > 0.914$ then $C_2^1 = 0.914$

$$C_2 = C_2^1 + M_2$$

$$M_P = 0.172 - 0.1550\alpha - 0.0016(t/\rho)$$

$$M_0 = 0.284 - 0.1780\alpha - 0.0046(t/\rho)$$

$$M_1 = -0.317 + 0.0115\alpha + 0.0099(t/\rho)$$

$$M_2 = 0.0045 + 0.2060\alpha - 0.0054(t/\rho)$$

$$C_3 = -0.45\left\{0.2 - \left(\frac{a}{t}\right)\right\}^{0.409}\left\{1.1 - \left(\frac{a}{c}\right)\right\}^{0.3}\left(\frac{L}{t}\right)^{-0.549}\left[1.0 - exp\left(-\left\{\frac{0.2 - \left(\frac{a}{t}\right)}{0.15}\right\}^2\right)\right] \quad \frac{a}{t} < 0.2$$

$$C_3 = 0 \quad \frac{a}{t} \geq 0.2$$

$$C_4 = -0.25\left\{0.03 - \left(\frac{a}{t}\right)\right\}^{1.28}\left\{1.1 - \left(\frac{a}{c}\right)\right\}^{0.285}\alpha^{1.5}\left(\frac{\rho}{t}\right)^{-0.7}\left(\frac{L}{t}\right)^{-0.394}\left[1.0 - exp\left(-\left\{\frac{0.03 - \left(\frac{a}{t}\right)}{S_4}\right\}^2\right)\right] \quad \frac{a}{t} < 0.03$$

where $S_4 = 0.006$, but $S_4 = 0.018$ if $\alpha > 0.6109$ and $\frac{\rho}{t} < 0.035$ and $\frac{L}{t} < 0.35$

$$C_4 = 0 \quad \frac{a}{t} \geq 0.03$$

Bending

$$Y_b = 0.96A\ ln\left(\frac{a}{t}\right) + C_0 + C_1\left(\frac{a}{t}\right) + C_2\left(\frac{a}{t}\right)^2 + C_3 + C_4 + C_5$$

$$A = -0.388 - 0.958\left(\frac{a}{c}\right)^{0.5} + 1.111\left(\frac{a}{c}\right) + M_A \quad \frac{a}{c} < 0.1$$

$$A = -0.686 + 0.310\left(\frac{a}{c}\right)^{0.5} + 0.0622\left(\frac{a}{c}\right) + M_A \quad \frac{a}{c} \geq 0.1$$

$$C_0 = 0.544 - 4.125\left(\frac{a}{c}\right)^{0.5} + 4.018\left(\frac{a}{c}\right) + M_0 \quad \frac{a}{c} < 0.1$$

$$C_0 = -0.645 + 1.111\left(\frac{a}{c}\right)^{0.5} - 0.648\left(\frac{a}{c}\right) + M_0 \quad \frac{a}{c} \geq 0.1$$

$$C_1 = -2.664 + 22.408\left(\frac{a}{c}\right)^{0.5} - 22.264\left(\frac{a}{c}\right) + M_1 \quad \frac{a}{c} < 0.1$$

$$C_1 = 3.860 - 6.128\left(\frac{a}{c}\right)^{0.5} + 2.876\left(\frac{a}{c}\right) + M_1 \quad \frac{a}{c} \geq 0.1$$

$$C_2 = 8.758 - 41.156\left(\frac{a}{c}\right)^{0.5} + 29.768\left(\frac{a}{c}\right) + M_2 \quad \frac{a}{c} < 0.1$$

$$C_2 = -1.648 + 0.926\left(\frac{a}{c}\right)^{0.5} + 0.00393\left(\frac{a}{c}\right) + M_2 \quad \frac{a}{c} \geq 0.1$$

$$M_A = 0.597 - 0.649\alpha - 0.0028(t/\rho)$$

$$M_0 = 1.282 - 1.325\alpha - 0.0077(t/\rho)$$

$$M_1 = -2.222 + 2.154\alpha + 0.0170(t/\rho)$$

$$M_2 = 0.789 - 0.621\alpha - 0.0097(t/\rho)$$

$$C_3 = -0.25\left\{0.25 - \left(\frac{a}{t}\right)\right\}^{0.5}\left\{1.1 - \left(\frac{a}{c}\right)\right\}^{0.16}\alpha^{2.0}\left(\frac{\rho}{t}\right)^{-0.16}\left(\frac{L}{t}\right)^{-0.37}\left[1.0 - exp\left(-\left\{\frac{0.25 - \left(\frac{a}{t}\right)}{0.15}\right\}^2\right)\right] \quad \frac{a}{t} < 0.25$$

$$C_3 = 0 \quad \frac{a}{t} \geq 0.25$$

$$C_4 = -4.0\left\{0.05 - \left(\frac{a}{t}\right)\right\}^{0.565}\left\{1.1 - \left(\frac{a}{c}\right)\right\}^{0.3}\alpha^{1.35}\left(\frac{\rho}{t}\right)^{-0.3}\left(0.455 - \left(\frac{L}{t}\right)\right)^{-0.204}\left[1.0 - exp\left(-\left\{\frac{0.05 - \left(\frac{a}{t}\right)}{S_4}\right\}^2\right)\right] \quad \frac{a}{t} < 0.05\ and\ \frac{L}{t} < 0.455$$

where $S_4 = 0.05$, but $S_4 = 0.06$ if $\alpha > 0.6109$ and $\frac{\rho}{t} < 0.04$ and $\frac{L}{t} < 0.35$

$$C_4 = 0.5\left\{0.05 - \left(\frac{a}{t}\right)\right\}^{1.1}\left\{1.1 - \left(\frac{a}{c}\right)\right\}^{-0.486}\alpha^{-2.66}\left(\frac{\rho}{t}\right)^{0.11}\left(\left(\frac{L}{t}\right) - 0.455\right)^{-0.0384}\left[1.0 - exp\left(-\left\{\frac{0.05 - \left(\frac{a}{t}\right)}{0.015}\right\}^2\right)\right] \quad \frac{a}{t} < 0.05 \; and \; \frac{L}{t} \geq 0.455$$

$$C_4 = 0 \quad \frac{a}{t} \geq 0.05$$

$$C_5 = -0.14\left\{\left(\frac{a}{t}\right) - 0.35\right\}^{0.098}\left\{1.1 - \left(\frac{a}{c}\right)\right\}^{0.862}\alpha^{0.675}\left(\frac{\rho}{t}\right)^{-0.077}\left(\frac{L}{t}\right)^{0.148}\left[1.0 - exp\left(-\left\{\frac{\left(\frac{a}{t}\right) - 0.35}{0.2}\right\}^2\right)\right] \quad \frac{a}{t} > 0.35$$

$$C_5 = 0 \quad \frac{a}{t} \leq 0.35$$

REFERENCES

[1] D. Radaj, C.M. Sonsino, W. Fricke, Fatigue assessment of welded joints by local approaches, Woodhead publishing, 2006.

[2] S. Zhang, Stress intensities at spot welds, International Journal of Fracture, 88 (1997) 167-185.

[3] A. Rupp, K. Störzel, V. Grubisic, Computer aided dimensioning of spot-welded automotive structures, (1995).

[4] S.D. Sheppard, M. Strange, Fatigue life estimation in resistance spot welds: initiation and early growth phase, Fatigue & Fracture of Engineering Materials & Structures, 15 (1992) 531-549.

[5] H. Kang, M. Barkey, Fatigue life estimation of spot welded joints using an interpolation/extrapolation technique, International Journal of Fatigue, 21 (1999) 769-777.

[6] H.T. Kang, Fatigue analysis of spot welds subjected to combined tension and shear loading, in, 1999.

[7] M.E. Barkey, H. Kang, Y.-L. Lee, Failure modes of single resistance spot welded joints subjected to combined fatigue loading, International Journal of Materials and Product Technology, 16 (2001) 510-527.

[8] H.T. Kang, Fatigue prediction of spot welded joints using equivalent structural stress, Materials & Design, 28 (2007) 837-843.

[9] H.T. Kang, P. Dong, J. Hong, Fatigue analysis of spot welds using a mesh-insensitive structural stress approach, International Journal of Fatigue, 29 (2007) 1546-1553.

[10] T. Nykänen, G. Marquis, T. Björk, Fatigue analysis of non-load-carrying fillet welded cruciform joints, Engineering Fracture Mechanics, 74 (2007) 399-415.

[11] M. Fermér, M. Andréasson, B. Frodin, Fatigue life prediction of MAG-welded thin-sheet structures, SAE Technical Paper, (1998).

[12] P. Dong, A structural stress definition and numerical implementation for fatigue analysis of welded joints, International Journal of Fatigue, 23 (2001) 865-876.

[13] O. Doerk, W. Fricke, C. Weissenborn, Comparison of different calculation methods for structural stresses at welded joints, International Journal of Fatigue, 25 (2003) 359-369.

[14] I. Poutiainen, P. Tanskanen, G. Marquis, Finite element methods for structural hot spot stress determination—a comparison of procedures, International Journal of Fatigue, 26 (2004) 1147-1157.

[15] K. Sripichai, K. Asim, J. Pan, Stress intensity factor solutions for estimation of fatigue lives of laser welds in lap-shear specimens, Engineering Fracture Mechanics, 78 (2011) 1424-1440.

[16] P. Paris, F. Erdogan, A Critical Analysis of Crack Propagation Laws, Journal of Basic Engineering, 85 (1963) 528-533.

[17] H. Petroski, J. Achenbach, Computation of the weight function from a stress intensity factor, Engineering Fracture Mechanics, 10 (1978) 257-266.

[18] H. Bueckner, Weight functions for the notched bar, ZAMM - Journal of Applied Mathematics and Mechanics/Zeitschrift für Angewandte Mathematik und Mechanik, 51 (1971) 97-109.

[19] X. Niu, G. Glinka, Theoretical and experimental analyses of surface fatigue cracks in weldments, in: Surface-Crack Growth: Models, Experiments, and Structures, ASTM International, 1990.

[20] X. Niu, G. Glinka, The weld profile effect on stress intensity factors in weldments, International Journal of Fracture, 35 (1987) 3-20.

[21] X. Niu, G. Glinka, Weight functions for edge and surface semi-elliptical cracks in flat plates and plates with corners, Engineering Fracture Mechanics, 36 (1990) 459-475.

[22] F. Brennan, W. Dover, R. Karé, A. Hellier, Parametric equations for T-butt weld toe stress intensity factors, International Journal of Fatigue, 21 (1999) 1051-1062.

[23] S. Maddox, Assessing the significance of flaws in welds subject to fatigue, Welding Journal, 53 (1974).

[24] Z. Wei, J. Hamilton, F. Yang, L. Luo, S. Lin, H. Kang, P. Dong, Comparison of Verity and Volvo Methods for Fatigue Life Assessment of Welded Structures, in, SAE Technical Paper, 2013.

[25] Y.-L. Lee, M.E. Barkey, H.-T. Kang, Metal fatigue analysis handbook, in, Elsevier, Oxford, 2012.

[26] HBM-nCode, DesignLife Theory Manuals, in, 2016.

[27] X. Wu, Z. Wei, H. Kang, A. Khosrovaneh, A Structural Stress Recovery Procedure for Fatigue Life Assessment of Welded Structures, in, SAE International, 2017.

[28] P. Dong, A robust structural stress procedure for characterizing fatigue behavior of welded joints, SAE Technical Paper, (2001).

[29] P. Dong, J. Hong, D. Osage, M. Prager, Fatigue of piping and vessel welds: ASME's FSRF rules revisited, in: ASME 2002 Pressure Vessels and Piping Conference, American Society of Mechanical Engineers, 2002, pp. 171-190.

[30] P. Dong, J. Hong, Z. Cao, Stresses and stress intensities at notches:'anomalous crack growth'revisited, International Journal of Fatigue, 25 (2003) 811-825.

[31] P. Dong, J. Hong, A. De Jesus, Analysis of recent fatigue data using the structural stress procedure in ASME Div. 2 Rewrite, in: Paper No. PVP2005-71511, Proceedings of ASME 2005 Pressure Vessel & Piping Conference, Denver, Colorado, July 17-21, ASME, 2005, pp. 253-261.

[32] H. Tada, P.C. Paris, G.R. Irwin, The stress analysis of cracks handbook, 1973.

[33] G. Shen, G. Glinka, Weight functions for a surface semi-elliptical crack in a finite thickness plate, Theoretical and Applied Fracture Mechanics, 15 (1991) 247-255.

[34] G.R. Irwin, Analysis of stresses and strains near the end of a crack traversing a plate, Journal of applied mechanics, 24 (1957) 361-364.

[35] T.L. Anderson, Fracture mechanics: fundamentals and applications, CRC Press, 2017.

[36] J. Newman Jr, I. Raju, Stress-intensity factor equations for cracks in three-dimensional finite bodies subjected to tension and bending loads, Computational methods in the mechanics of fracture, 2 (1986) 311-334.

[37] X. Wang, S. Lambert, Weight functions and stress intensity factors for semi-elliptical cracks in T-plate welded joints, Fatigue & Fracture of Engineering Materials & Structures, 21 (1998) 99-117.

[38] J.J. Bonnen, R. Mandapati, H. Kang, R.M. Iyengar, A. Khosrovaneh, M.A. Amaya, K. Citrin, H.-C. Shih, Durability of advanced high strength steel gas metal arc welds, SAE International Journal of Materials & Manufacturing, 2 (2009) 155-171.

[39] A. Moftakhar, G. Glinka, Calculation of stress intensity factors by efficient integration of weight functions, Engineering Fracture Mechanics, 43 (1992) 749-756.

[40] N.E. Dowling, Mean stress effects in stress-life and strain-life fatigue, in, SAE Technical Paper, 2004.

[41] N. Dowling, C. Calhoun, A. Arcari, Mean stress effects in stress-life fatigue and the Walker equation, Fatigue & Fracture of Engineering Materials & Structures, 32 (2009) 163-179.

[42] K.N. Smith, T.H. Topper, P. Watson, A stress-strain function for the fatigue of metals, Journal of Materials, 5 (1970) 767-778.

[43] H.-T. Kang, X. Wu, Structural Stress Correction Methods for Linear Elastic Finite Element Analysis of Spot Welded Joints, in: ASME 2016 International Mechanical Engineering Congress and Exposition, American Society of Mechanical Engineers, 2016, pp. V009T012A048-V009T012A048.

PUBLICATIONS

[1] X. Wu, Z. Wei, H. Kang, A. Khosrovaneh, A Structural Stress Recovery Procedure for Fatigue Life Assessment of Welded Structures, in, SAE International, 2017.

[2] H.-T. Kang, X. Wu, A. Khosrovaneh, Z. Li, Data Processing Procedure for Fatigue Life Prediction of Spot-Welded Joints Using a Structural Stress Method, in: Z. Wei, K. Nikbin, P.C. McKeighan, D.G. Harlow (Eds.) Fatigue and Fracture Test Planning, Test Data Acquisitions and Analysis, 2017, pp. 198-211.

[3] H.-T. Kang, X. Wu, Structural Stress Correction Methods for Linear Elastic Finite Element Analysis of Spot Welded Joints, in: ASME 2016 International Mechanical Engineering Congress and Exposition, American Society of Mechanical Engineers, 2016, pp. V009T012A048-V009T012A048.

[4] Z. Wei, S. Das, R. Barr, G. Rohrs, R. Rebandt, X. Wu, H. Kang, Development of Lightweight Hanger Rods for Vehicle Exhaust Applications, in, SAE International, 2017.